

## TARGET-BASED ANTICANCER GLYCYRRHETINIC DERIVATIVES: DESIGN, SYNTHESIS, BIOLOGICAL ASSESSMENT AND MOLECULAR DOCKING STUDIES

Gaber O. Moustafa<sup>1\*</sup>, Atef Kalmouch<sup>1</sup>, Somaia S. Abd El-Karim<sup>2</sup>, Eman S. Nossier<sup>3,4</sup>, Marwa M. Mounier<sup>5</sup>, Heba El- Sayed<sup>6</sup>, Abdulrahman A. Almehizia<sup>7</sup>, Ahmed M. Naglah<sup>7</sup> and Amer A. Zen<sup>8</sup>

<sup>1</sup>Peptide Chemistry Department, Chemical Industries Research Institution, National Research Centre, 12622-Dokki, Cairo, Egypt

<sup>2</sup>Department of Therapeutic Chemistry, National Research Centre, Dokki, Cairo 12622, Egypt

<sup>3</sup>Department of Pharmaceutical Medicinal Chemistry and Drug Design Department, Faculty of Pharmacy (Girls), Al-Azhar University, Cairo, 11754, Egypt

<sup>4</sup>The National Committee of Drugs, Academy of Scientific Research and Technology, Cairo, 11516, Egypt

<sup>5</sup>Pharmacognosy Department, Pharmaceutical and Drug Industries Research Division, National Research Centre, 33 El Bohouth St., Dokki, Giza, P.O. Box 12622, Egypt

<sup>6</sup>Botany and Microbiology Department, Faculty of Science, Helwan University, Egypt

<sup>7</sup>Department of Pharmaceutical Chemistry, College of Pharmacy, King Saud University, P.O. Box 2457, Riyadh 11451, Saudi Arabia

<sup>8</sup>Chemistry & Forensics Department, Clifton Campus, Nottingham Trent University, Nottingham NG11 8NS, UK

(Received February 26, 2024; Revised May 13, 2024; Accepted May 15, 2024)

**ABSTRACT.** 18-Glycyrrhetic acid (GA) is regarded as the principal active component isolated from the Chinese medicinal plant of licorice root, and it has considerable anticancer actions. This work was built on the discovery and design of brand-new 18-glycyrrhetic acid (GA) amino acid peptides and peptide ester analogs. The cytotoxic evaluation exhibited that despite the promising cytotoxic activity of the tested peptides **2**, **3**, **4**, **6**, and **7** in *MCF-7* and *HCT-116* cancer cells, with  $IC_{50}$  values ranging from 5.1-7.4 and 6.6-72.7  $\mu\text{g/mL}$ , respectively. Furthermore, all freshly produced GA-peptides with moderate to high activity on tumor cell lines produced a favorable safety profile versus typical human dermal fibroblasts (BJ-1) cellular lineage. Interestingly, **2**, **4** and **6** demonstrated excellent multitargeting inhibitory profiles against CDK-2, VEGFR-2, and PDGFR- $\alpha$  kinases. Moreover, since peptide **6** was the most active cytotoxic agent, it was chosen as an illustrative candidate to examine its influence on many apoptotic markers in invitro studies, including Bax, caspase-3 and 7, DNA fragmentation, Bcl-2, p53, and tubulin polymerization inhibition. All novel analogs were tested for their antimicrobial efficacy versus a panel of microbial strains. The peptide **6** was also subjected to molecular docking simulations in the active sites of the prior kinases.

**KEY WORDS:** Peptides, Glycyrrhetic acid, Anticancer, Cytotoxicity, Molecular docking, Antimicrobial activity

## INTRODUCTION

18-Glycyrrhetic acid is a pentacyclic triterpene of the oleanane type found mostly in the root of the Chinese plant Licorice (*Glycyrrhiza glabra*) [1, 2]. Various findings have reported that GA and its byproducts produce different pharmacological effects, such as bronchodilator, detoxification, anti-inflammatory, antitumor, antiulcer, antimicrobial, and antiviral functions [3, 4]. Recently, the antiproliferative activity of GA has been extensively investigated in breast-ovarian cancers, hepatoma, leukemia, and Gastric tumor cells [5, 6].

\*Corresponding authors. E-mail: gosman79@gmail.com

This work is licensed under the Creative Commons Attribution 4.0 International License

It has been shown that GA exerts its potent anticancer impact by disrupting the actin cytoskeleton, hence inhibiting angiogenesis [7, 8] along with impairing the p38 MAPK-AP1 signaling axis [9] as well as an immunomodulatory effect through suppression of COX-2 and its enzymatic product PGE-2, which have been reported to display crucial roles in the development of cancer disease [10]. In addition, mechanistic studies represented that the GA-based cytotoxic activity is correlated with the mitochondrial apoptotic pathway via potential depolarization of the mitochondrial membrane, which consequently results in the upregulation of caspase-9, caspase-3 and activation of the production of reactive oxygen species (ROS) as well as causing a balance between pro-proteins and anti-apoptotic proteins, leading to apoptosis [11]. Many studies have been carried out in the last decades to modify the GA backbone, aiming to improve its anticancer effectiveness, such as ring A, ring C, and C-30 carboxylic acid modifications [12]. In addition, hybridization of GA was also performed with other biological moieties of pronounced cytotoxic activity, including “cinnamide, triphenylphosphonium, and Rhodamine B” [13]. Numerous semi-synthetic oleanolic acid analogs, for example, the CDDO and CDDO-Me with conjugation of 1-en-2-cyano-3-oxo moiety to ring A, were discovered to be the most efficient anticancer drugs and have undergone clinical studies. (Figure 1A) [14]. Likewise, GA similar compound CDODA-Me displayed potent antitumor activity (Figure 1A) [15, 16]. COOTO-Meanalogue displayed a strong suppression of cancer cell proliferation and activation of apoptosis in conjunction with decreased (HDAC) histone deacetylase protein levels [17].

Amino acids are the basic material that sustains biological life and play vital functions. Different pharmacological actions, including anticancer activity, are shown by amino acids, which are extremely water soluble [18]. Despite the wide spectrum of the biological activities related to natural products, the low bioavailability and poor solubility are considered their major disadvantages [19]. Interestingly, conjugation with amino acid residues might increase the bioavailability features and ADME qualities of the natural product. These characteristics distinguish amino acids as the primary natural structural enhancers [18].

Inspired by the preceding discoveries and in keeping with our prior studies in the area of identification of novel effective anticancer and antibacterial compounds [20-29], this manuscript represented the development and formulation of novel 18 $\beta$ -glycyrrhetic amide derivatives of potential anticancer activities. The synthetic strategy was based on coupling GA with different amino acids at its C-30 carboxylic group. In addition, esterification of the hydroxyl group of ring A with substituted glycine derivatives was also carried out, aiming to improve the anticancer potentiality of the new derivatives and to explore the structure–activity relationship (Figure 1B).

The cytotoxic potential of all produced compounds was evaluated versus three human cancer cell lines: (*MCF-7*) breast cancer, (*HCT-116*) colon cancer, and (*HepG-2*) liver cancer. Since different studies related the anticancer activity of various macrocycles to different enzyme inhibitions that have been involved in carcinogenesis cases such as CDK-2, VEGFR-2, PDGFR- $\alpha$ , JAK-2, FLT-3 and EGFR, representing them as successful attractive targets for anticancer therapies [30], it was of interest in this study to examine the GA-peptides which exhibited the most promising anticancer activity 2, 4 and 6 as multitargeting kinase inhibitors against various kinases such as CDK-2, VEGFR-2, PDGFR- $\alpha$ . In addition, further evaluation was also carried out for the promising peptide 6 against different oncogenic parameters such as (TubB) tubulin polymerization, p53, Bax, Bcl-2, caspase-3 and 7, and % fragmentation of DNA to find out its cytotoxic mechanism-based. Since peptide 6 exhibited the most promising multitargeting kinase inhibitory action, a molecular modeling investigation was conducted to justify its promising pharmacological impact by elucidating its mechanisms of binding with the building blocks of proteins residues of the examined kinases CDK-2, VEGFR-2, and PDGFR. It has been documented that specific infections are primarily responsible for various forms of cancer [31]. Many cytotoxic antibiotics, such as “Actinomycin, Adriamycin/Doxorubicin”, and certain other compounds, exert their effects by causing damage to DNA and simultaneously triggering the host's existing defense mechanisms. This process is considered one of the key pathways through

which such chemotherapeutic agents exert their antimicrobial effects [32]. Consequently, there was a keen interest in investigating the antimicrobial effectiveness of the recently synthesized GA-peptides. This research aimed to develop new, safer agents with dual capabilities, serving as both potent anticancer and antimicrobial agents of natural origin.

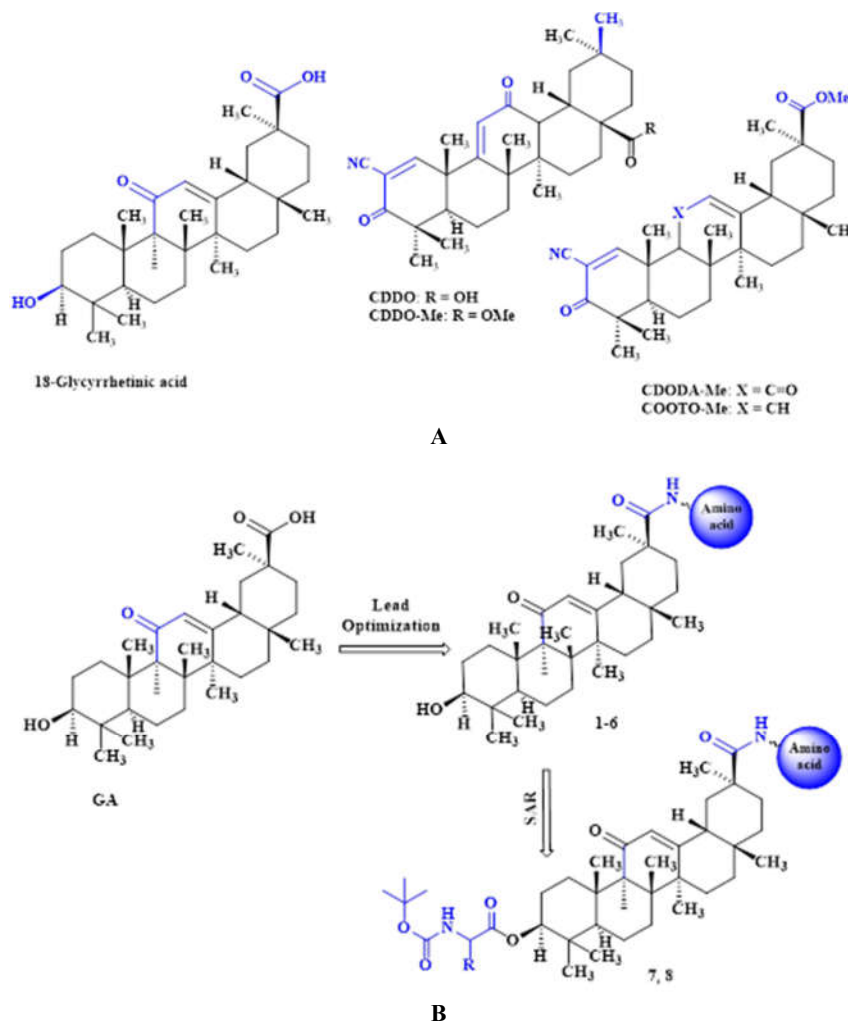


Figure 1. **A:** The chemical makeup of GA and many semi-artificial pentacyclic triterpenoids. **B:** Design of new GA-peptides 1-8 of potential anticancer activity.

## EXPERIMENTAL

### Chemistry

Melting points were determined in an “Electro Thermal” Digital melting point apparatus (Shimadzu, Tokyo, Japan) (model: IA9100). The solvents, chemicals, and thin layer

chromatography used in this work were obtained from international chemical companies: Sigma (Ronkonkoma, NY, USA), Fluka (Buchs, Switzerland), and E. Merck (Hohenbrunn, Germany). The melting points were determined using the digital electrothermal melting point apparatus in opened glass capillary tubes and are uncorrected. Elemental micro-analyses for carbon, nitrogen, and hydrogen (Micro-Analytical Unit, Cairo University, Cairo, Egypt) were obtained within good limits of the theoretical values ( $\pm 0.4\%$ ). Infrared (IR) spectra were listed as KBr disks using the Fourier transform infrared spectrophotometer (Shimadzu; Model: IR affinity-1S) at the Micro-Analytical Unit at Cairo University in Egypt. The measurements of mass spectra occurred on a gas chromatograph-mass spectrometer (Shimadzu, Kyoto, Japan; Model: QP2010ultra) at the Micro-analytical Unit at Cairo University in Egypt. The  $^1\text{H-NMR}$  and  $^{13}\text{C-NMR}$  spectra were run on JEOL, JöEL500 MHz instruments (Tokyo, Japan) in  $\text{DMSO-d}_6$ .

Synthesis of amino acid ester hydrochlorides and Boc-protected amino acids were prepared according to the general method described by Curtius and Goebel [26] and [27], respectively.

*Synthesis of ethyl 2-(2-(10-hydroxy-2,4a,6a,6b,9,9,12a-heptamethyl-13-oxo-1,2,3,4,4a,5,6,6a,6b,7,8,8a,9,10,11,12,12a,12b,13,14b-icosahydricene-2-carboxamido)acetamido)acetate (1).* Yield: 60; m.p. 160-162  $^\circ\text{C}$ . IR ( $\text{cm}^{-1}$ ): (KBr): 3650 (OH primary cyclic alcohol), 3408 (NH stretching), 2933 (CH aliphatic), 1752 (C=O ester), 1659, 1535 and 1457 (C=O amide I, amide II and amid III), 1382, 1334 ( $\text{CH}_2$  aliphatic), 1252, 1195 ( $\text{CH}_3$  aliphatic).  $^1\text{H-NMR}$  (500 MHz,  $\delta$ , ppm,  $\text{DMSO-d}_6$ ):  $\delta$ : 8.21-7.19 (s, 2H, CONH,  $\text{D}_2\text{O}$  exchangeable), 5.40 (s, 1H, COCH=C, GL moiety), 5.00 (s, 1H, OH, GL moiety), 4.00-3.38 (s, 4H, 2  $\text{CH}_2$  and q, 2H, O  $\text{CH}_2$   $\text{CH}_3$ , Gly), 2.85-2.45 (t, 4H, 3CH and s, CH, GL moiety), 1.94-1.72 (16H, t, 6  $\text{CH}_2$ , m,  $\text{CH}_2$ , d,  $\text{CH}_2$ , GL moiety), 1.44 (t, 3H, O  $\text{CH}_2$   $\text{CH}_3$ , Gly), 1.05-0.80 (s, 21H, 7  $\text{CH}_3$ , GL moiety). MS (EI, 70 eV):  $m/z$  (%) = 613 ( $\text{M}^+$ , 36.36%), 612 (60.84%), 610 (44.06%), 548 (82.52%), 428 (86.71%), 135 (90.21%), 71 (100%), 50 (48.95%). Molecular formula (M.wt.),  $\text{C}_{36}\text{H}_{56}\text{N}_2\text{O}_6$  (612.8). Calculated analysis; C, 70.55; H, 9.21; N, 4.57. Found; C, 70.50; H, 9.14; N, 4.51.

*Synthesis of 2-(2-(10-hydroxy-2,4a,6a,6b,9,9,12a-heptamethyl-13-oxo-1,2,3,4,4a,5,6,6a,6b,7,8,8a,9,10,11,12,12a,12b,13,14b-icosahydricene-2-carboxamido)acetamido)acetic acid (2).* Yield: 80; m.p. 207-209  $^\circ\text{C}$ . IR ( $\text{cm}^{-1}$ ): (KBr): 3610 (OH primary cyclic alcohol), 3509 (OH acid), 3429 (NH stretching), 2943, 2869 (CH aliphatic), 1705 (C=O acid), 1655, 1531 and 1458 (C=O amide I, amide II and amid III), 1386, 1326 ( $\text{CH}_2$  aliphatic), 1283, 1256, 1212 ( $\text{CH}_3$  aliphatic).  $^1\text{H-NMR}$  (500 MHz,  $\delta$ , ppm,  $\text{DMSO-d}_6$ ):  $\delta$ : 12.57 (s, 1H, OH, Gly), 8.12-7.73 (s, 2H, CONH,  $\text{D}_2\text{O}$  exchangeable), 5.53, 5.51 (s, 1H, COCH=C, GL moiety) and (s, 1H, OH, GL moiety), 4.35-4.20 (s, 4H, 2  $\text{CH}_2$ , Gly), 3.05-2.75 (t, 4H, 3CH and s, CH, GL moiety), 1.90-1.75 (16H, t, 6  $\text{CH}_2$ , m,  $\text{CH}_2$ , d,  $\text{CH}_2$ , GL moiety), 1.15-0.90 (s, 21H, 7  $\text{CH}_3$ , GL moiety). MS (EI, 70 eV):  $m/z$  (%) = 586 ( $\text{M}^+ + 1$ , 34.21%), 585 ( $\text{M}^+$ , 34.21%), 584 (72.63%), 583 (32.63%), 479 (100%), 233 (66.32%), 172 (78.95%), 50 (46.84%). Molecular formula (M.wt.),  $\text{C}_{34}\text{H}_{52}\text{N}_2\text{O}_6$  (584.8). Calculated analysis; C, 69.83; H, 8.96; N, 4.79. Found; C, 69.81; H, 8.92; N, 4.75.

*Synthesis of methyl 2-(2-(2-(10-hydroxy-2,4a,6a,6b,9,9,12a-heptamethyl-13-oxo-1,2,3,4,4a,5,6,6a,6b,7,8,8a,9,10,11,12,12a,12b,13,14b-icosahydricene-2-carboxamido)acetamido)acetamido)-3-(tritylthio)propanoate (3).* Yield: 65; m.p. 77-79  $^\circ\text{C}$ .  $[\alpha]_{\text{D}}^{25}$ : +136.22 (C, 0.02,  $\text{DMSO}$ ). IR ( $\text{cm}^{-1}$ ): (KBr): 3526 (OH primary cyclic alcohol), 3397 (NH stretching), 3056 (CH aromatic), 2936, 2870 (CH aliphatic), 1743 (C=O ester), 1645 and 1447 (C=O amide I and amide II), 1385, 1321 ( $\text{CH}_2$  aliphatic), 1231 ( $\text{CH}_3$  aliphatic).  $^1\text{H-NMR}$  (500 MHz,  $\delta$ , ppm,  $\text{DMSO-d}_6$ ):  $\delta$ : 8.95, 8.94 (s, 3H, CONH,  $\text{D}_2\text{O}$  exchangeable), 8.21-7.93 (15H, aromatic H, Trityl moiety), 5.45 (s, 1H, COCH=C, GL moiety), 5.35 (s, 1H, OH, GL moiety), 4.40-4.30 (s, 4H, 2  $\text{CH}_2$ , Gly), 3.55 (s, 3H, O  $\text{CH}_3$ , S-Trityl-LCys), 3.80 (t, CH, S-Trityl-LCys), 3.00 (d,  $\text{CH}_2$ , S-Trityl-LCys), 2.95-2.70 (t, 4H, 3CH and s, CH, GL moiety), 1.80-1.40 (16H, t, 6  $\text{CH}_2$ , m,  $\text{CH}_2$ , d,  $\text{CH}_2$ , GL moiety), 1.14-0.85 (s, 21H, 7  $\text{CH}_3$ , GL moiety). MS (EI, 70 eV):  $m/z$  (%) = 945 ( $\text{M}^+ + 1$ , 29.47%), 944 ( $\text{M}^+$ ,

35.69%), 942 (4.10%), 929 (61.20%), 855 (100%), 598 (54.20%), 266 (39.65%), 50 (9.68%). Molecular formula (M.wt.), C<sub>57</sub>H<sub>73</sub>N<sub>3</sub>O<sub>7</sub>S (944.3). Calculated analysis; C, 72.50; H, 7.79; N, 4.45; S, 3.40. Found; C, 72.47; H, 7.79; N, 4.43; S, 3.42.

*Synthesis of 2-(2-(2-(10-hydroxy-2,4a,6a,6b,9,9,12a-heptamethyl-13-oxo-1,2,3,4,4a,5,6,6a,6b,7,8,8a,9,10,11,12,12a,12b,13,14b-icosahydricene-2-carboxamido)acetamido)acetamido)-3-(tritylthio)propanoic acid (4).* Yield: 71; m.p. 255-257 °C. [ $\alpha$ ]<sub>D</sub><sup>25</sup>: + 75.00 (C, 0.02, DMSO). IR (cm<sup>-1</sup>): (KBr): 3600 (OH primary cyclic alcohol), 3500 (OH acid), 3423 (NH stretching), 3058 (CH aromatic), 2937, 2869 (CH aliphatic), 1710 (C=O acid), 1654 and 1449 (C=O amide I and amide II), 1384, 1317 (CH<sub>2</sub> aliphatic), 1254, 1210 (CH<sub>3</sub> aliphatic). <sup>1</sup>H-NMR (500 MHz,  $\delta$ , ppm, DMSO-d<sub>6</sub>):  $\delta$ : 12.43 (s, 1H, OH, S-Trityl-LCys), 8.32-7.86 (s, 3H, CONH, D<sub>2</sub>O exchangeable), 7.43-6.97 (15H, aromatic H, Trityl moiety), 5.55 (s, 1H, COCH=C, GL moiety), 5.14 (s, 1H, OH, GL moiety), 4.38-4.25 (s, 4H, 2 CH<sub>2</sub>, Gly), 3.70 (t, CH, S-Trityl-LCys), 3.55 (s, 3H, O CH<sub>3</sub>, S-Trityl-LCys, disappeared), 3.05 (d, CH<sub>2</sub>, S-Trityl-LCys), 2.90-2.55 (t, 4H, 3CH and s, CH, GL moiety), 1.90-1.45 (16H, t, 6 CH<sub>2</sub>, m, CH<sub>2</sub>, d, CH<sub>2</sub>, GL moiety), 1.04-0.90 (s, 21H, 7 CH<sub>3</sub>, GL moiety). MS (EI, 70 eV): m/z (%) = 931 M<sup>+</sup>+1, 29.67%), 930 (M<sup>+</sup>, 64.59%), 929 (41.63%), 825 (60.77%), 593 (89.95%), 569 (100%), 418 (75.60%), 218 (72.25%), 52 (33.97%). Molecular formula (M.wt.), C<sub>56</sub>H<sub>71</sub>N<sub>3</sub>O<sub>7</sub>S (930.2). Calculated analysis; C, 72.30; H, 7.69; N, 4.52; S, 3.45. Found; C, 72.26; H, 7.63; N, 4.50; S, 3.41.

*Synthesis of ethyl 1-(10-hydroxy-2,4a,6a,6b,9,9,12a-heptamethyl-13-oxo-1,2,3,4,4a,5,6,6a,6b,7,8,8a,9,10,11,12,12a,12b,13,14b-icosahydricen-2-yl)-1,4,7,10,13-pentaoxo-9-(tritylthiomethyl)-2,5,8,11,14-pentaazahexadecan-16-oate (5).* Yield: 65; m.p. 88-90 °C. [ $\alpha$ ]<sub>D</sub><sup>25</sup>: + 112.00 (C, 0.02, ethanol). IR (cm<sup>-1</sup>): (KBr): 3650 (OH primary cyclic alcohol), 3380 (NH stretching), 3100 (CH aromatic), 2944, 2920 (CH aliphatic), 1720 (C=O ester), 1670, 1582 and 1495 (C=O amide I, amide II and amide III), 1380 (CH<sub>2</sub> aliphatic), 1262, 1217 (CH<sub>3</sub> aliphatic). <sup>1</sup>H-NMR (500 MHz,  $\delta$ , ppm, DMSO-d<sub>6</sub>):  $\delta$ : 8.63-8.54 (s, 5H, CONH, D<sub>2</sub>O exchangeable), 8.47-7.74 (15H, aromatic H, Trityl moiety), 5.55 (s, 1H, COCH=C, GL moiety), 5.14 (s, 1H, OH, GL moiety), 4.65-4.50 (s, 8H, 4 CH<sub>2</sub>, Gly), 4.40-4.30 (q, 2H, O CH<sub>2</sub> CH<sub>3</sub>, Gly), 3.95 (t, CH, S-Trityl-LCys), 3.85 (s, 3H, O CH<sub>3</sub>, S-Trityl-LCys, disappeared), 3.22 (d, CH<sub>2</sub>, S-Trityl-LCys), 2.95-2.70 (t, 4H, 3CH and s, CH, GL moiety), 2.00-1.50 (16H, t, 6 CH<sub>2</sub>, m, CH<sub>2</sub>, d, CH<sub>2</sub>, GL moiety), 1.35 (t, 3H, O CH<sub>2</sub> CH<sub>3</sub>, Gly), 1.15-0.90 (s, 21H, 7 CH<sub>3</sub>, GL moiety). MS (EI, 70 eV): m/z (%) = 1073 (M<sup>+</sup> +1, 12.60%), 1072 (M<sup>+</sup>, 25.08%), 633 (100%), 507 (50.50%), 300 (20.46%), 50 (0.92%). Molecular formula (M.wt.), C<sub>62</sub>H<sub>81</sub>N<sub>5</sub>O<sub>9</sub>S (1072.4). Calculated analysis; C, 69.44; H, 7.61; N, 6.53; S, 2.99. Found; C, 69.50; H, 7.60; N, 6.50; S, 2.88.

*Synthesis of 1-(10-hydroxy-2,4a,6a,6b,9,9,12a-heptamethyl-13-oxo-1,2,3,4,4a,5,6,6a,6b,7,8,8a,9,10,11,12,12a,12b,13,14b-icosahydricen-2-yl)-1,4,7,10,13-pentaoxo-9-(tritylthiomethyl)-2,5,8,11,14-pentaazahexadecan-16-oic acid (6).* Yield: 52; m.p. 282-284 °C. [ $\alpha$ ]<sub>D</sub><sup>25</sup>: + 212.00 (C, 0.02, DMSO). IR (cm<sup>-1</sup>): (KBr): 3630 (OH primary cyclic alcohol), 3525 (OH acid), 3425 (NH stretching), 3058 (CH aromatic), 2951 (CH aliphatic), 1716 (C=O acid), 1652 and 1450 (C=O amide I and amide II), 1385, 1326 (CH<sub>2</sub> aliphatic), 1210 (CH<sub>3</sub> aliphatic). <sup>1</sup>H-NMR (500 MHz,  $\delta$ , ppm, DMSO-d<sub>6</sub>):  $\delta$ : 12.14 (s, 1H, OH, Gly), 8.12-6.83 (s, 5H, CONH, D<sub>2</sub>O exchangeable) and (15H, aromatic H, Trityl moiety), 5.40 (s, 1H, COCH=C, GL moiety), 5.04 (s, 1H, OH, GL moiety), 4.54-4.30 (s, 8H, 4 CH<sub>2</sub>, Gly), 3.80 (t, CH, S-Trityl-LCys), 3.65 (s, 3H, O CH<sub>3</sub>, S-Trityl-LCys, disappeared), 3.00 (d, CH<sub>2</sub>, S-Trityl-LCys), 2.85-2.60 (t, 4H, 3CH and s, CH, GL moiety), 1.90-1.30 (16H, t, 6 CH<sub>2</sub>, m, CH<sub>2</sub>, d, CH<sub>2</sub>, GL moiety), 0.95-0.82 (s, 21H, 7 CH<sub>3</sub>, GL moiety). MS (EI, 70 eV): m/z (%) = 1044 (M<sup>+</sup>, 19.86%), 1043 (35.27%), 1041 (53.42%), 898 (62.67%), 554 (100%), 293 (94.52%), 90 (86.30%), 50 (41.44%). Molecular formula (M.wt.), C<sub>60</sub>H<sub>77</sub>N<sub>5</sub>O<sub>9</sub>S (1044.3). Calculated analysis; C, 69.00; H, 7.43; N, 6.71; S, 3.07. Found; C, 68.98; H, 7.41; N, 6.70; S, 3.04.

*Synthesis of ethyl 1-(10-(2-(2-(tert-butoxycarbonylamino)acetamido)acetoxo)-2,4a,6a,6b,9,9,12a-heptamethyl-13-oxo-1,2,3,4,4a,5,6,6a,6b,7,8,8a,9,10,11,12,12a,12b,13,14b-icosahydro-picen-2-yl)-1,4,7,10,13-pentaaxo-9-(tritylthiomethyl)-2,5,8,11,14-pentaazahexadecan-16-oate (7).* Yield: 74; m.p. 99-101 °C.  $[\alpha]_D^{25}$ : + 200.11 (C, 0.02, ethanol). IR (cm<sup>-1</sup>): (KBr): 3328 (NH stretching), 2929 (CH aromatic), 2853 (CH aliphatic), 1716 (C=O ester), 1628, 1575, 1532 and 1444 (C=O amide I, amide II, amid III and amid IV), 1384, 1310 (CH<sub>2</sub> aliphatic), 1245, 1203 (CH<sub>3</sub> aliphatic). <sup>1</sup>H-NMR (500 MHz, δ, ppm, DMSO-d<sub>6</sub>): δ: 8.94-6.80 (s, 7H, CONH, D<sub>2</sub>O exchangeable) and (15H, aromatic H, Trityl moiety), 5.70 (s, 1H, COCH=C, GL moiety), 5.16 (s, 1H, OH, GL moiety, disappeared), 4.80-4.30 (s, 12H, 6 CH<sub>2</sub>, q, 2H, O CH<sub>2</sub> CH<sub>3</sub>, Gly), 4.62-4.42), 3.95 (t, CH, S-Trityl-LCys), 3.84 (s, 3H, O CH<sub>3</sub>, S-Trityl-LCys, disappeared), 2.90 (d, CH<sub>2</sub>, S-Trityl-LCys), 2.72-2.55 (t, 4H, 3CH and s, CH, GL moiety), 1.85-1.55 (16H, t, 6 CH<sub>2</sub>, m, CH<sub>2</sub>, d, CH<sub>2</sub>, GL moiety), 1.30-1.20 (s, 9H, 3 CH<sub>3</sub>, Boc moiety, t, 3H, O CH<sub>2</sub> CH<sub>3</sub>, Gly), 0.90-0.80 (s, 21H, 7 CH<sub>3</sub>, GL moiety). MS (EI, 70 eV): m/z (%) = 1286 (M<sup>+</sup>, 1.02%), 1087 (24.07%), 1038 (52.78%), 980 (60.37%), 652 (100%), 185 (48.06%), 67 (39.81%), 53 (8.70%). Molecular formula (M.wt.), C<sub>71</sub>H<sub>95</sub>N<sub>7</sub>O<sub>13</sub>S (1286.6). Calculated analysis; C, 66.28; H, 7.44; N, 7.62; S, 2.49. Found; C, 66.19; H, 7.41; N, 7.66; S, 2.50.

*Synthesis of ethyl 1-(10-(2-(tert-butoxycarbonylamino)-4-methylpentanoyloxy)-2,4a,6a,6b,9,9,12a-heptamethyl-13-oxo-1,2,3,4,4a,5,6,6a,6b,7,8,8a,9,10,11,12,12a,12b,13,14b-icosahydro-picen-2-yl)-1,4,7,10,13-pentaaxo-9-(tritylthiomethyl)-2,5,8,11,14-pentaazahexadecan-16-oate (8).* Yield: 50; m.p. 209-211 °C.  $[\alpha]_D^{25}$ : + 100.00 (C, 0.02, ethanol). IR (cm<sup>-1</sup>): (KBr): 3625 (OH primary cyclic alcohol), 3370 (NH stretching), 3112 (CH aromatic), 2933, 2905 (CH aliphatic), 1745 (C=O ester), 1654, 1595 and 1490 (C=O amide I, amide II and amide III), 1388 (CH<sub>2</sub> aliphatic), 1290, 1210 (CH<sub>3</sub> aliphatic). <sup>1</sup>H-NMR (500 MHz, δ, ppm, DMSO-d<sub>6</sub>): δ: 9.02-6.95 (s, 6H, CONH, D<sub>2</sub>O exchangeable) and (15H, aromatic H, Trityl moiety), 5.65 (s, 1H, COCH=C, GL moiety), 4.80 (q, 1H, CHNH, L-Leu), 4.70-4.47 (s, 8H, 4 CH<sub>2</sub>, Gly), 4.35-4.24 (q, 2H, O CH<sub>2</sub> CH<sub>3</sub>, Gly), 4.00 (t, CH, S-Trityl-LCys), 3.85 (s, 3H, O CH<sub>3</sub>, S-Trityl-LCys, disappeared), 3.35 (d, CH<sub>2</sub>, S-Trityl-LCys), 3.00-2.80 (t, 4H, 3CH and s, CH, GL moiety), 1.95 (t, 2H, CH<sub>2</sub>, L-Leu), 1.85-1.45 (16H, t, 6 CH<sub>2</sub>, m, CH<sub>2</sub>, d, CH<sub>2</sub>, GL moiety), 1.35 (t, 1H, CH (CH<sub>3</sub>)<sub>2</sub>, L-Leu), 1.20 (t, 3H, O CH<sub>2</sub> CH<sub>3</sub>, Gly), 1.15-0.95 (s, 21H, 7 CH<sub>3</sub>, GL moiety), 0.90-0.75 (d, 6H, CH<sub>3</sub>, L-Leu). MS (EI, 70 eV): m/z (%) = 1286 (M<sup>+</sup>, 5.00%), 1096 (32.15%), 613 (33.50%), 366 (100%), 271 (20.40%), 50 (4.00%). Molecular formula (M.wt.), C<sub>73</sub>H<sub>100</sub>N<sub>6</sub>O<sub>12</sub>S (1285.7). Calculated analysis; C, 68.20; H, 7.84; N, 6.54; S, 2.49. Found; C, 68.14; H, 7.80; N, 6.58; S, 2.50.

### Biological activities

#### Cytotoxic assay

Human breast MCF-7, colon HCT-116 and liver HepG-2 carcinoma cell line were taken from Vacsera (Giza, Egypt). The culture was retained in RPMI 1640 medium with 1% antibiotic-antimycotic mixture (25 µg/mL amphotericin B, 10,000 µg/mL streptomycin sulfate and 10,000U/mL potassium penicillin), 1% L-glutamine, and complemented by 10% heat inactivated fetal bovine serum. The culturing and subculturing were done according to [33]. Doxorubicin was used as a positive control and DMSO as a negative control. This experiment was carried out according to the reported MTT assay method and the absorbance was measured at 595 nm.

#### Kinase assays

The activities of the examined compounds against CDK-2, EGFR and PDGFR-α were *in vitro* tested using CDK4 ELISA kit, Cloud-Clone Corp for CDK4, USAbcam's Human In cell ELISA Kit (ab 126419) for EGFR and ADP-GloTM Kinase Assay for PDGFR-α, respectively. The procedures of the used kits were done according to the manufacturer's instructions.

*Estimation of Bcl2 level*

The samples and standards having Bcl-2 were estimated as previously mentioned [34]. Addition of biotin-conjugated antibody was followed by streptavidin-HRP. Then the reaction was terminated by adding acid and the absorbance was measured at 450 nm.

*Estimation of Bax level*

The levels of Bax protein were evaluated according to the reported method [35]. Addition of monoclonal antibody specific to Bax captured on the plate was followed by incubation and addition of Streptavidin conjugated to Horseradish peroxidase. Then the reaction was terminated by adding acid and optical density of the produced color was measured at 450 nm.

*Estimation of human p53 level*

The samples or standard having human p53 binds to antibodies adsorbed to the microwells. Addition of biotin-conjugated was followed by incubation and addition of dispense of unbound biotin-conjugated streptavidin HRP. Then the reaction was terminated by adding acid and the absorbance was measured at 450 nm [36].

*Calculation of IC<sub>50</sub> values*

The IC<sub>50</sub> values were estimated for the promising active compounds using the SPSS computer program (SPSS for windows, statistical analysis software package /version 9/ 1989 SPSS Inc., Chicago, USA) and utilizing probit analysis.

*Human CASP7 (Caspase 7) Estimation*

The micro ELISA plate provided in this kit pre-coated with CASP7 specific antibody. A biotinylated CASP7 antibody and Avidin-Horseradish Peroxidase (HRP) conjugate was added. Aspire the excess components. The substrate solution was added. Wells that contain CASP7, biotinylated detection antibody and Avidin-HRP conjugate will appear blue in color. The color turns yellow followed the addition of sulphuric acid solution. The optical density (OD) was measured at a wavelength of 450 nm ± 2 nm [37].

*Human CASP-3 (Caspase-3) Estimation*

Activity of caspase-3 was assessed using Caspase-Glo 3 kit (Promega Corporation · 2800 Woods Hollow Road · Madison, WI 53711-5399 USA) according to the manufacturer's instructions and previously mentioned procedure [37].

*Enzyme-linked Immunosorbent Assay Kit for Tubulin Beta (TubB)*

The MCF-7 cells were inoculated using RPMI 1640 (supplemented with 1% penicillin-streptomycin and 10% FBS) at concentration 10,000 cells/well. For 24 hours before the enzyme assay of Tubulin, the tested compounds were added, followed by addition of Avidin conjugated to Horseradish Peroxidase (HRP) to each microplate well and incubated. After addition of TMB substrate solution, the wells containing TUBb, enzyme-conjugated Avidin and biotin-conjugated antibody revealed a change in color. Addition of sulphuric acid solution terminated the enzymatic reaction. The color change was measured spectrophotometrically at a wavelength of 450 nm ± 10 nm [38].

*Estimation of DNA Fragmentation through DPA assay*

Assessment of DNA fragmentation of the cells was done, as described by the reported method [39]. Briefly, the cells were lysed for 15 min on ice with 0.5% (v/v) Triton X-100, 20 mM EDTA

and 5  $\mu\text{M}$  Tris (pH 8.0). Then, the cells were centrifuged to separate intact chromatin from DNA fragments for 20 min, at 27,000 Xg. Measurement of the amount of DNA was done using a diphenylamine reagent and the optical density was measured at 600 nm.

#### *In-vitro antimicrobial activity*

*Antimicrobial* activity of the tested chemical peptides was determined by well diffusion method for pathogenic bacteria having Gram- positive bacteria (*Staphylococcus aureus* ATCC25923, *Streptococcus pneumonia* and *Micrococcus luteus*) and Gram- negative bacteria (*Escherichia coli* ATCC25922, *Pseudomonas aeruginosa* ATCC7853 and *Proteus sp.*) and *Candida albicans* as human pathogen yeast using well diffusion method [40, 41].

#### *Molecular docking study*

The 2D structure of the newly synthesized derivatives **6** was drawn through ChemDraw. The protonated 3D was employed using standard bond lengths and angles, using molecular operating environment (MOE-Dock) software version 2014.0901 [42, 43]. Then, the geometry optimization and energy minimization were applied to get the Conf Search module in MOE, followed by saving of the MOE file for upcoming docking process. The co-crystallized structures of CDK-2, VEGFR-2 and PDGFR- $\alpha$  kinases with their ligands PY8, sorafenib and imatinib were downloaded (PDB codes: 2J9M, 4ASD and 6JOL, respectively) [42, 43] from protein data bank. All minimizations were performed using MOE until an RMSD gradient of  $0.05 \text{ kcal}\cdot\text{mol}^{-1}\text{\AA}^{-1}$  with MMFF94x force field and the partial charges were automatically calculated. Preparation of the enzyme structures was done for molecular docking using Protonate 3D protocol with the default options in MOE. London dG scoring function and Triangle Matcher placement method were used in the docking protocol. At the first, validation of the docking processes were established by docking of the native ligands, followed by docking of the derivative **6** within the ATP-binding sites after elimination of the co-crystallized ligands.

## RESULTS AND DISCUSSION

### *Chemistry*

New target peptides (**1-8**) have been synthesized according to Schemes 1 and 2. GA has been conjugated with many amino acids. These coupling reactions were carried out using conventional synthetic peptide methods (in solution) [6, 21, 24].

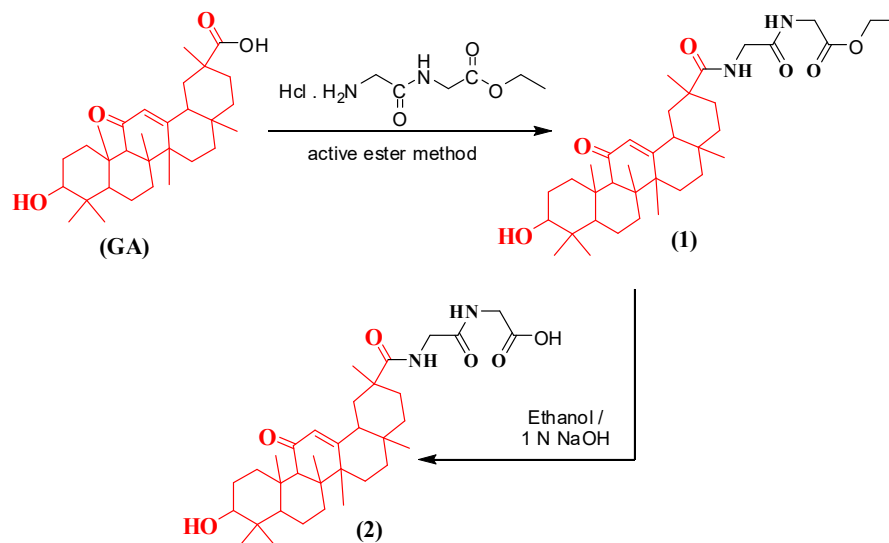
### *Biological evaluations*

#### *In vitro anticancer action*

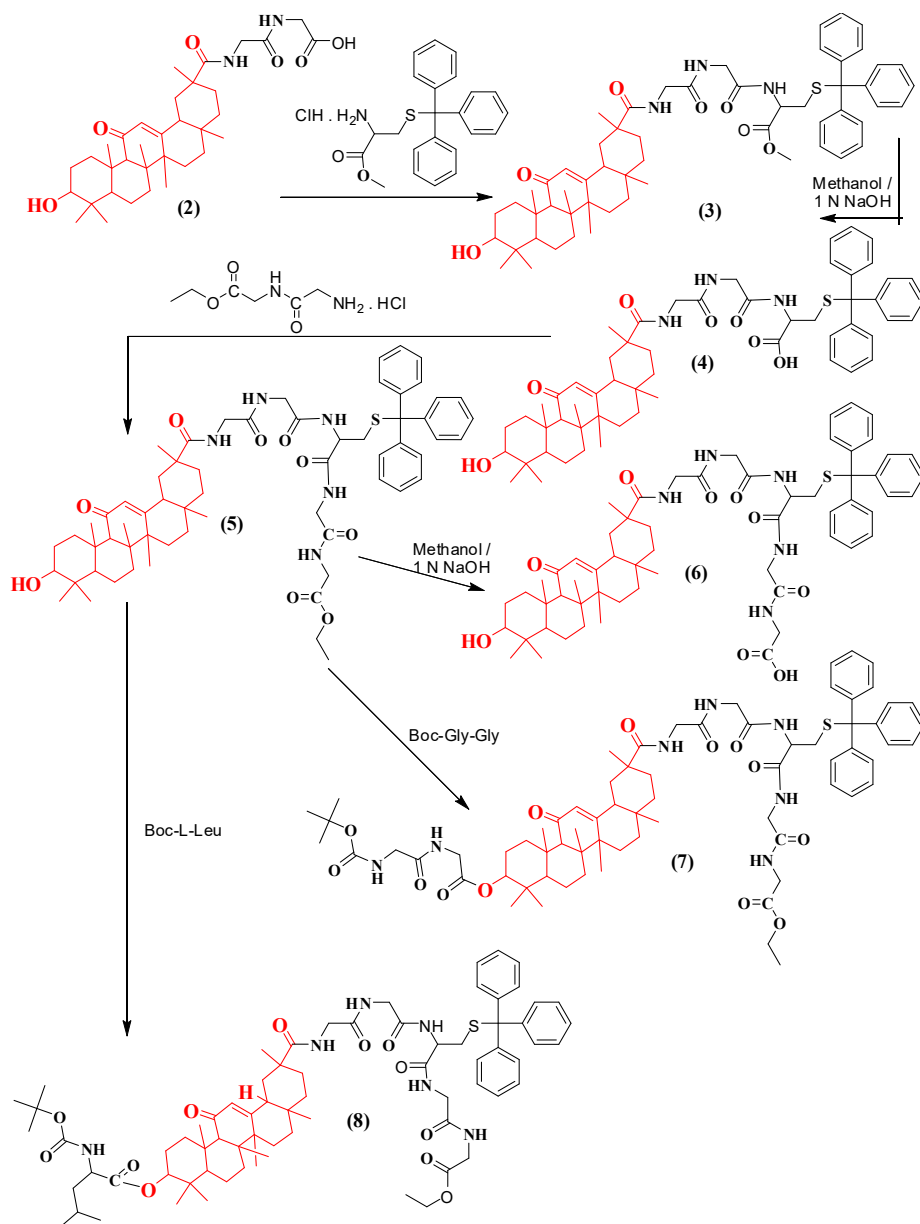
In this study, all the new target peptides **1-8** were initially screened for their cytotoxic action versus three human cancer cell lines, namely *MCF-7*, *HCT-116*, colon carcinoma, and *HepG2* at a starting concentration of 10  $\mu\text{g}/\text{mL}$  via using MTT assay. The resulting data are depicted in Figure 2A. It has been found that the tested peptides **2**, **3**, **6**, **7**, and **4** possessed the highest cytotoxic activity against the breast tumor cells (*MCF-7*) with cytotoxicity percentages of 98.6, 98.1, 97.7, 95.2 and 86.4 %, correspondingly. On the contrary, compound **1** showed a moderate cytotoxic effect, and derivatives **5** and **8** presented low activity. Similarly, compounds **6**, **2**, **3**, **4**, and **7** represented the most promising cytotoxic effect against the colon tumor cells (*HCT-116*) with growth inhibition percentages 99.1, 97.7, 97.3, 95.3 and 89.2 %, respectively. Conversely, compounds **1**, **5**, and **8** showed weak activity. Furthermore, with respect to the examined hepatocellular carcinoma cells (*HepG-2*), compound **6** was the only promising derivative showing tumor growth inhibition of 97%. Compounds **2** and **4** showed moderate activity, with growth inhibition percentages of 58.9 and 56.4 %, respectively, while the rest of the compounds possessed weak cytotoxic potency (Figure 2A).

Afterward, all the compounds that showed moderate to high cytotoxic capabilities were further screened versus the typical human dermal cell lineage (Bj-1) to identify the safety of these tested peptides. As shown in Figure 2B, all the tested peptides represented a promising safety profile against the tested normal cells. GA-peptides **1**, **2**, **3**, **4**, **6**, and **7** exhibited cytotoxic activity ranging from 0.1- 22.9%.

In order to investigate their median growth inhibitory concentrations ( $IC_{50}$ s), all the compounds that represented cytotoxic activity over 70% inhibition of the tested cancer cells were subjected to the dose-dependent MTT assay at varying concentrations (0.625, 1.25, 2.5, 5 and 10  $\mu\text{g/mL}$ ), taking doxorubicin as a standard drug. Thus, GA-peptides **2**, **3**, **4**, **6**, and **7** were investigated as anticancer agents against their respective human cancer cell lines “breast *MCF-7*, colon *HCT-116*, and liver *HepG-2* cell lines” at different concentrations (0.625, 1.25, 2.5, 5 and 10  $\mu\text{g/mL}$ ). The results were conveyed as  $IC_{50}$  values ( $\mu\text{g/mL}$ ) and depicted in Table 1 (Figure 2C). According to the biological results in Table 1, it could be noted that the conjugation of glycyglycine peptide **2** with the glycyglycyl-S-tritylcysteinate moiety as the peptides **3**, **4**, and **6** retained the potent cytotoxic activity. The glycyglycine peptide **6** exhibited two-fold higher growth inhibition activity against *MCF-7* than the standard drug doxorubicin, with  $IC_{50}$  values of 6.2 and  $13 \pm 1$   $\mu\text{g/mL}$ , respectively. On the other hand, compound **6** was slightly less active than doxorubicin against *HCT-116*, with  $IC_{50}$  values of  $6.60 \pm 0.11$  and  $2.00 \pm 3$   $\mu\text{g/mL}$ , respectively. A detectable drop in the activity of compound **6** was recorded against *HepG-2* compared to the reference drug, with  $IC_{50}$  values of  $63.73 \pm 0.21$  and 1.00  $\mu\text{g/mL}$ , correspondingly. Also, the cytotoxicity of compounds **3** and **4** was approximately two-fold higher than that obtained by doxorubicin against *MCF-7*, with  $IC_{50}$  values of  $6.32 \pm 0.15$  and  $7.40 \pm 0.05$   $\mu\text{g/mL}$ , respectively. Compound **4** exhibited a small drop in potency against *HCT-116* with an  $IC_{50}$  value of  $7.11 \pm 0.10$   $\mu\text{g/mL}$ . In contrast, compound **3** produced a significant drop in potency compared to the reference drug with an  $IC_{50}$  value of  $53.82 \pm 0.20$   $\mu\text{g/mL}$ . Although the glycyglycyl-S-tritylcysteinate-OMe peptide **7** has maintained its activity against *MCF-7* cancer cells with an  $IC_{50}$  value of 6.22  $\mu\text{g/mL}$ , its activity remarkably decreased against *HCT-116* with an  $IC_{50}$  value of 72.73  $\mu\text{g/mL}$ . Unfortunately, all the tested peptides were inactive against *HepG-2* cancer cells, while compound **6** was moderately active with an  $IC_{50}$  value of 63.73  $\mu\text{g/mL}$  (Table 1).



Scheme 1. Synthetic routes for peptide derivatives based on glycyrrhetic acid (**1**, **2**).



Scheme 2. Synthetic routes for peptide derivatives based on glycyrrhetic acid (3-8).

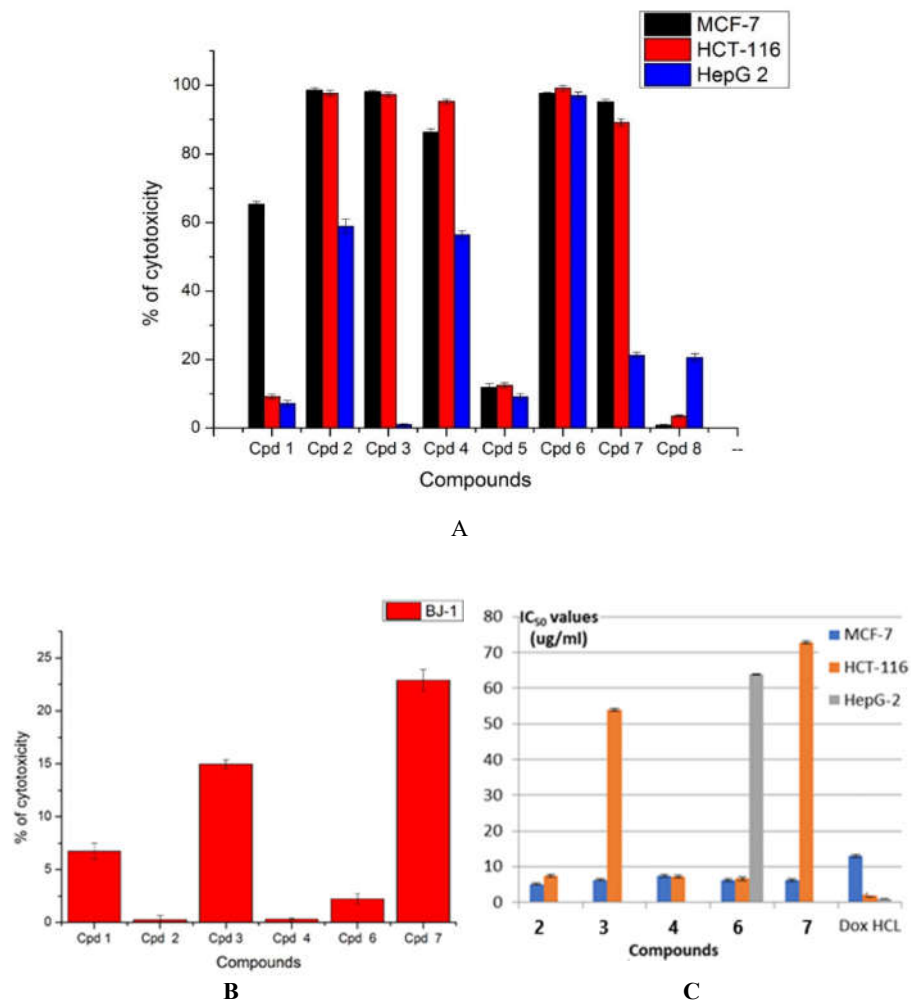


Figure 2. **A:** The cytotoxicity percentages of the new eight GA-peptides against (MCF-7) human breast carcinoma, (HCT-116) human colon carcinoma, and (HepG-2) hepatocellular carcinoma at 10  $\mu\text{g/mL}$ . Each result is an average of triplicate,  $\pm$  standard deviation. **B:** The cytotoxicity percentages of the active compounds against the human normal skin cell line (BJ-1) at 10  $\mu\text{g/mL}$ . Each result is an average of triplicate  $\pm$  standard deviation. **C:** IC<sub>50</sub> values of GA-peptides 2-4, 6, and 7 against various human cancer cell lines  $\pm$  standard deviation.

It could be noted that all the assessed peptides, the glycyL-glycine peptide 2 and its *S*-trityl-L-cysteine analogs 3, 4, 6, and 7, appeared to be potent cytotoxic candidates against the human breast cancer cells (*MCF-7*) as related to the standard drug as doxorubicin HCL. Alternatively, the *O*-methylated derivatives (3, 7) observed a detectable decrease in potency, which were moderately active against *HCT-116* cancer cells. In contrast, the other analogs (2, 4, and 6)

retained their potent activity against *HCT-116* cancer cells. This result could be explained by the fact that the presence of free hydroxyl groups is preferable for cytotoxic activity because they act as H donors to bind with the active sites of the ligands' sites. It could be observed that the conjugation of the *tert*-butoxycarbonyl)leucine moiety at ring A as compound **7** did not enhance the potency against *MCF-7* and might be a reason for the detectable decrease in the activity towards *HCT-116* cancer cells due to the steric hindrance that might occur, preventing the molecular structure from having a good fit with the target protein on which they act. The hepatic carcinoma cells (*HepG-2*) were insensitive towards the evaluated GA-peptides except peptide **6**, which produced moderate activity.

Table 1. The IC<sub>50</sub> estimates for GA-based peptides vs. several cancer cell lines.

| Compd. No.         | IC <sub>50</sub> (µg/mL) ± SD |                |               |
|--------------------|-------------------------------|----------------|---------------|
|                    | <i>MCF-7</i>                  | <i>HCT-116</i> | <i>HepG-2</i> |
| <b>2</b>           | 5.11±0.01                     | 7.41±0.03      | ----          |
| <b>3</b>           | 6.32±0.15                     | 53.82±0.20     | ----          |
| <b>4</b>           | 7.40±0.05                     | 7.11±0.10      | ----          |
| <b>6</b>           | 6.20±0.25                     | 6.60±0.11      | 63.73±0.21    |
| <b>7</b>           | 6.22±0.12                     | 72.73±0.10     | ----          |
| <b>Doxorubicin</b> | 13.00 ± 0.10                  | 2.00 ± 0.31    | 1.00 ± 0.10   |

IC<sub>50</sub>: The concentration of a substance that suppresses cellular survival by half; every value is the average of 3 repeats ± SD.

#### *In vitro enzymatic assays*

It has been reported that the enzymes (CDK-2) cyclin-dependent kinase-2, (VEGFR-2) vascular endothelial growth factor receptor, and platelet-derived growth factor receptor - $\alpha$  (PDGFR- $\alpha$ ) play significant roles in tumor cell proliferation, survival, differentiation, angiogenesis, and apoptosis. Accordingly, they are considered successful targets for anticancer therapies, particularly for gaining multitargeting anticancer drugs of improved activity [44]. Thus, it was of interest to determine the enzymatic inhibitory efficacy of the most promising cytotoxic GA-peptides with the safest profile against the normal cells (BJ1) **2**, **4**, and **6** against a panel of three different kinases: CDK-2, VEGFR-2, and PDGFR- $\alpha$  using the multitarget inhibitor staurosporine as a standard drug. The resultant data were tabulated in Table 2. It could be observed that glycyglycine peptide **6** represented the most promising inhibitory effect against the three examined kinases. It represented a suppressing activity against CDK-2 that was about 2-fold higher than the reference drug, with IC<sub>50</sub> values of 0.074 µM and 0.150 µM, respectively. Furthermore, peptide **6** appeared to be approximately equipotent to staurosporine against both VEGFR-2 and PDGFR- $\alpha$  with IC<sub>50</sub> values of 0.024 and 0.051 µM and IC<sub>50</sub> staurosporine; 0.030 and 0.040 µM, respectively. Although the other two tested peptides **2** and **4** exhibited promising suppression impact against the three examined enzymes with IC<sub>50</sub> values ranging from 2.640 to 6.125 µM, they appeared much less potent than the standard drug staurosporine. The data obtained increased understanding of the pharmacological mechanisms of the glycyglycine peptide **6**, indicating that the suppression impact of CDK-2, VEGFR-2, and PDGFR- $\alpha$  could be considered one of the anticancer mechanisms that it relied on. In contrast, the anticancer activity of the other two peptides, **2** and **4**, was primarily based on other modes of action.

#### *The effect of the GA-peptide 6 on Bax, Bcl-2, Bax/Bcl-2 ratio and p53 levels*

The Bcl-2 protein is essential in tumor growth and suppressed cell apoptotic intrinsic process [45]. Unlike, the pro-apoptotic Bax induces apoptosis inside the cell [46]. It has been reported that cell survival through apoptosis inhibition is enhanced by raising the amount of the anti-apoptotic Bcl-2 in the cancer cells, leading to apoptosis [44]. The fate of the cell is determined by the balance

among Bax and Bcl-2 proteins [44]. Additionally, p53 is a tumor suppressor transcription factor protein. This protein is commonly mutated in human cancers and expressed in many biological stressors, including DNA damage [47] and [48]. The p53 pathway was reported to either arrest the cell cycle or apoptotic cascades through the mRNA copies of Bcl-2 and Bax genes [48].

Table 2. Kinase inhibitory assessment of the promising derivatives **2**, **4**, and **6** (IC<sub>50</sub> in  $\mu\text{M}$ ) against CDK-2, VEGFR-2, and PDGFR- $\alpha$  enzymes.

| Compound             | IC <sub>50</sub> (Mean $\pm$ SEM) ( $\mu\text{M}$ ) |                  |                  |
|----------------------|-----------------------------------------------------|------------------|------------------|
|                      | CDK-2                                               | VEGFR-2          | PDGFR- $\alpha$  |
| <b>2</b>             | 5.741 $\pm$ 0.05                                    | 6.125 $\pm$ 0.05 | 2.725 $\pm$ 0.15 |
| <b>4</b>             | 3.955 $\pm$ 0.01                                    | 5.220 $\pm$ 0.10 | 2.640 $\pm$ 0.12 |
| <b>6</b>             | 0.074 $\pm$ 0.15                                    | 0.024 $\pm$ 0.25 | 0.051 $\pm$ 0.20 |
| <b>Staurosporine</b> | 0.150 $\pm$ 0.12                                    | 0.030 $\pm$ 0.10 | 0.040 $\pm$ 0.01 |

IC<sub>50</sub>: The concentration of a substance that suppresses cellular survival by half; every value is the average of 3 repeats  $\pm$  SEM.

Based on the promising results referring to the anticancer activity of peptide **6**, it was of interest to study its various pathways, such as its influence on the apoptotic-induced pathway, including P53 and Bax apoptotic proteins, BCL-2 anti-apoptotic proteins, the BAX/Bcl-2 proportion, tubulin polymerization inhibition, fragmentation of DNA, and caspase-7 induction.

Using peptide **6** at its IC<sub>50</sub> concentration of 6.2  $\mu\text{g}/\text{mL}$  for 24 hours reduced the anti-apoptotic protein Bcl-2 from 7.2 to 4.1  $\text{ng}/\text{mL}$  compared to the typical *MCF-7* cells, but less potently than doxorubicin, which decreased Bcl-2 concentrations to 0.40  $\text{ng}/\text{mL}$ . In addition, compound **6** increased the amount of Bax protein from 65.5 to 259.4  $\text{pg}/\text{mL}$  compared to typical *MCF-7* cells, which was comparable to the level attained by doxorubicin, which was 259.2. Accordingly, peptide **6** led to a predictable elevation in the Bax/BCL-2 ratio, supporting its efficacy in elevating the therapeutic response in *MCF-7* cells (Figures 3-A and 3-B). In addition, compound **6** increased the amount of p53 in treated *MCF-7* cells by roughly 9.8-fold, from 111.  $\text{pg}/\text{mL}$  to 1090 compared to the typical untreated cells.

*Impact of GA-peptide 6 on the quantities of caspase-3 and 7, the assembly of tubulin (TubB), and the percentage of fragmentation of the DNA*

All apoptosis events involve shrinking cell size, consolidation of chromatin, and fragmentation of the DNA, requiring the association of caspase-7, which is considered a marker of cell apoptosis. Caspases, or cysteine-dependent aspartate-specific proteases, constitute a family of enzymes that are essential for initiating and executing the apoptosis process within a cell. Treating the *MCF-7* cells with an IC<sub>50</sub> value of 6.2  $\mu\text{g}/\text{mL}$  of peptide **6** for 24 hours increased the level of caspase-7 as compared to unsubjected cells from 0.3 to 1.4  $\text{ng}/\text{mL}$ , similar to doxorubicin, which elevated the caspase-7 level to 1.9  $\text{ng}/\text{mL}$  (Figure 3C). In addition, peptide **6** has raised the level of caspase-3 from about 0.3  $\text{ng}/\text{mL}$  in the control *MCF-7* cells to 0.90  $\text{ng}/\text{mL}$  in the cells subjected, while the reference drug doxorubicin raised the caspase-3 level to a higher level of 1.90  $\text{ng}/\text{mL}$  (Figure 3D). Furthermore, peptide **6** has also had a profound influence on DNA fragmentation levels in the treated *MCF-7* cells. It increased the ratio of fragmentation of the DNA from 7.8% in the control untreated *MCF-7* cells to reach to approximately 25.4% in the peptide 6-treated *MCF-7* cells. The reference drug colchicine appeared to be more effective, producing a DNA fragmentation percentage of 40.7 %, as shown in (Figure 3E). In addition, peptide **6** has had a profound influence on the DNA fragmentation rate of treated *MCF-7* cells. It increased the percentage level of DNA fragmentation from 7.8% in the control, untreated *MCF-7* cells to approximately 25.4% in the peptide 6-treated *MCF-7* cells. The reference drug colchicine appeared to be more effective, producing a DNA fragmentation percentage of 40.7 percent, as shown in (Figure 3E).

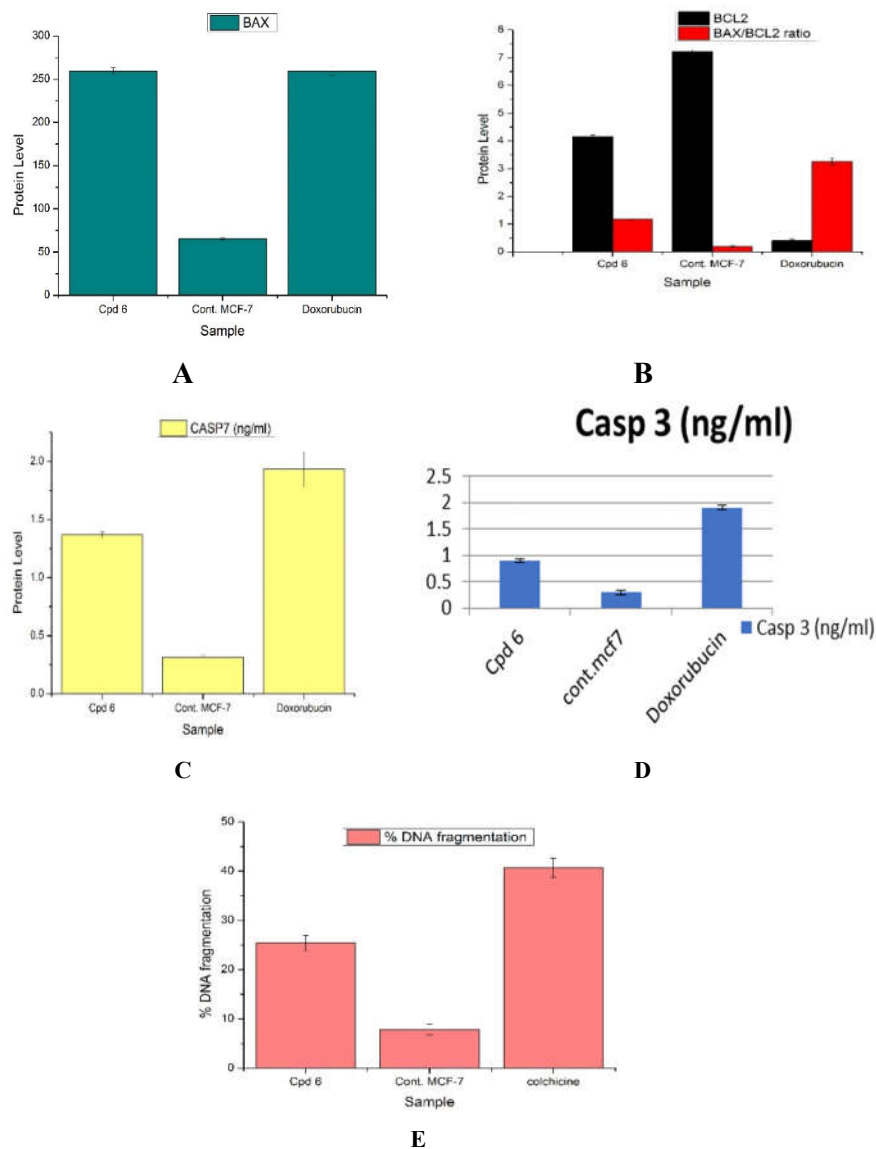


Figure 3. **A:** Bax protein levels in breast cells treated with compound **6**, typical cells, and cells subjected with the standard drug doxorubicin  $\pm$  standard deviation. **B:** Protein levels of Bcl2 and Bax/Bcl2 proportion in MCF-7 treated cells with compound **6**, typical MCF-7 cells (as control), and doxorubicin treated MCF-7 cells. **C:** Caspase-7 protein levels of treated cells with compound **6** compared with untreated cells and doxorubicin treated cells  $\pm$  standard deviation. **D:** Caspase 7 protein levels of treated cells with compound **6** compared with untreated cells and doxorubicin treated cells  $\pm$  standard deviation. **E:** % of DNA fragmentation in compound **6**-treated cells compared to untreated and colchicine-treated cells  $\pm$  standard deviation.

Furthermore,  $\alpha$ - and  $\beta$ -tubulins polymerize to generate polarized filaments, which are known as microtubules, which are essential for a multiple of cellular activities, such as cell division, morphology, and intracellular transport [49]. Accordingly, the identification of new inhibitors is still an active area of anticancer research [50]. Accordingly, the effect of peptide **6** was also studied against tubulin B. The resultant data showed that  $IC_{50}$  of peptide **6** on *MCF-7* is 14886.5 ng/mL for 24 h while the reference drug colchicine reaches 487.7 ng/mL, which implicates that peptide **6** was not potent enough to suppress tubulin B as the reference drug colchicine. GA-peptide **6** appears to be a powerful pro-apoptotic candidate by activating the intrinsic mitochondrial route of apoptosis.

#### Antimicrobial activity

The recently synthesized peptides 1-4, 6, and 7 (disregarding compounds **5** and **8**) underwent assessment as potential antimicrobial candidates against a set of pathogenic gram-positive bacteria, namely “*Staphylococcus aureus* ATCC25923, *Streptococcus pneumoniae* RCMB 010010, and *Micrococcus luteus*, as well as three pathogenic gram-negative bacteria: *Escherichia coli* ATCC25922, *Pseudomonas aeruginosa* ATCC7853, and *Proteus vulgaris* RCMB 010085, in addition to the yeast *Candida albicans*”. This evaluation was conducted using the well diffusion method [40]. Gentamycin and ketoconazole were employed as reference substances for assessing antibacterial and antifungal activities, respectively. The data obtained for each analog was recorded as the mean size of the inhibitory zones (IZ) in millimeters, representing the area where microorganism inhibition of growth occurred close to the discs (see Table 3).

It is evident that all the tested analogs of GA displayed stronger inhibitory activity against *Micrococcus luteus* compared to gentamicin, with inhibition zones ranging from 25 to 30 mm, while gentamicin had an IZ of  $24.4 \pm 0.72$  mm. While ordinarily innocuous, it may become an opportunity-based pathogen and has been related with a number of illnesses, including but not limited to meningitis, septic arthritis, and endocarditis [41]. In contrast, all of the chemicals studied showed very mild action versus the fungal and microbial strains used in the study, with inhibition zone ranges of 12-17 mm, in contrast to ketoconazole, which had an IZ of  $22.8 \pm 0.10$  mm, and gentamicin, which exhibited IZ ranges of 12-19 mm, compared to its reference range of 20-27 mm.

Table 3. Displays the results of the antimicrobial effectiveness assessment for the recently created compounds, employing the well diffusion assay technique.

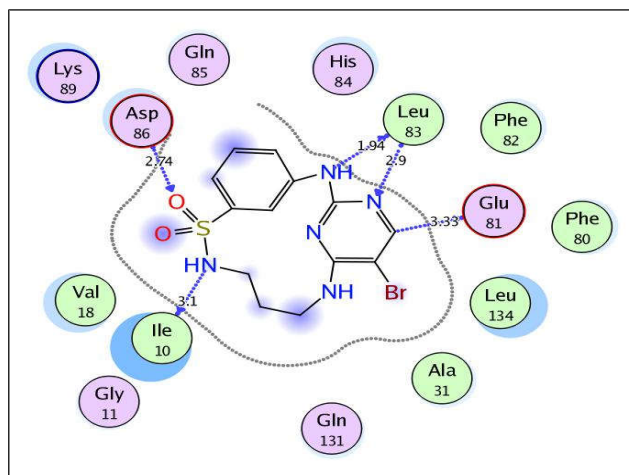
| Pathogenic microbial Strains |                                                           | Diameter of inhibition zone (mm) |         |         |         |         |         |             |             |
|------------------------------|-----------------------------------------------------------|----------------------------------|---------|---------|---------|---------|---------|-------------|-------------|
|                              |                                                           | 1                                | 2       | 3       | 4       | 6       | 7       | GM          | KC          |
| Gram-positive bacteria       | <i>Staphylococcus aureus</i> ATCC25923                    | 15±0.16                          | 17±0.16 | 12±0.23 | 13±0.16 | 12±0.21 | 13±0.21 | 27.2 ± 0.80 | -           |
|                              | <i>Streptococcus pneumoniae</i> RCMB 010010               | 15±0.13                          | 17±0.16 | 15±0.21 | 15±0.21 | 15±0.16 | 14±0.21 | 25.4 ±0.18  | -           |
|                              | <i>Micrococcus luteus</i>                                 | 30±0.21                          | 30±0.15 | 25±0.13 | 25±0.31 | 28±0.72 | 28±0.16 | 24.4 ±0.72  | -           |
| Gram-negative bacteria       | <i>Escherichia coli</i> ATCC25922                         | 20±0.06                          | 16±0.31 | 17±0.21 | 15±0.16 | 15±0.23 | 12±0.13 | 26.3 ± 0.15 | -           |
|                              | <i>Pseudomonas aeruginosa</i> ATCC7853                    | 18±0.23                          | 15±0.16 | 16±0.23 | 15±0.21 | 19±0.23 | 14±0.31 | 24.41±0.18  | -           |
|                              | <i>Proteus vulgaris</i> RCMB 010085<br><i>Proteus sp.</i> | -                                | 17±0.21 | 12±0.23 | -       | 13±0.13 | 10±0.23 | 20.0 ± 0.30 | -           |
| Yeast                        | <i>Candida albicans</i>                                   | -                                | 12±0.22 | 11±0.23 | 17±0.21 | 14±0.23 | -       |             | 22.8 ± 0.10 |

GM: gentamicin; KC: ketoconazole.

*Molecular docking study on CDK-2, VEGFR-2, and PDGFR- $\alpha$* 

The objective of the docking study was to gain a deeper understanding of how the promising derivative **6** binds to the ATP binding sites of CDK-2, VEGFR-2, and PDGFR- $\alpha$  kinases, including their binding orientations and modes. In order to conduct this docking experiment, we integrated the “Molecular Operating Environment (MOE-Dock) software, specifically version 2014.0901” [42, 43]. To ensure the reliability of our docking process, we validated it by performing redocking experiments of co-crystallized ligands PY8, sorafenib, and imatinib within the active sites of CDK-2, VEGFR-2, and PDGFR- $\alpha$ . These co-crystallized ligands are associated with the respective protein structures with PDB codes 2J9M, 4ASD, and 6JOL [42, 43]. The results of the redocking revealed energy scores of -10.25, -12.44, and -11.20 kcal/mol for CDK-2, VEGFR-2, and PDGFR- $\alpha$ , respectively, along with small RMSD values of 0.68 Å, 0.81 Å, and 1.12 Å, indicating a close alignment among docked ligands and their locations in co-crystals.

The native ligand, PY8 was depicted in the vicinity of CDK-2 through five H-bond forces; two were formed between sulfonamide moiety the backbones of Ile10 and Asp86 (distance: 3.10 and 2.74 Å, respectively) and the other H-bonds was between the aminopyrimidine scaffold and the backbone of Glu81 and Leu83 (distance: 3.33, 1.94 and 2.90 Å, respectively) (Figure 4A). Within the binding site of VEGFR-2, the ligand sorafenib illustrated two H-bonds between the urea group and the essential amino acids Asp1046 and Glu885 (distance: 2.79 and 2.58 Å, respectively). On the other hand, the pyridine nitrogen and the carbamoyl proton exhibited two hydrogen bonds with the backbone of Cys919 (distance: 3.10 and 2.88 Å, respectively) (Figure 4B). Moreover, there were arene-cation interactions with Asp1046 and Phe1047. Regarding the PDGFR- $\alpha$  receptor, imatinib formed several H-bonds with Met648, Thr674, Cys677, Val815, His816, and Asp836 (distance: 3.45, 3.00, 2.88, 3.14, 2.98 and 2.94 Å, respectively), and arene-cation interactions with Leu599, Val607 and Phe837 (Figure 4C).



A

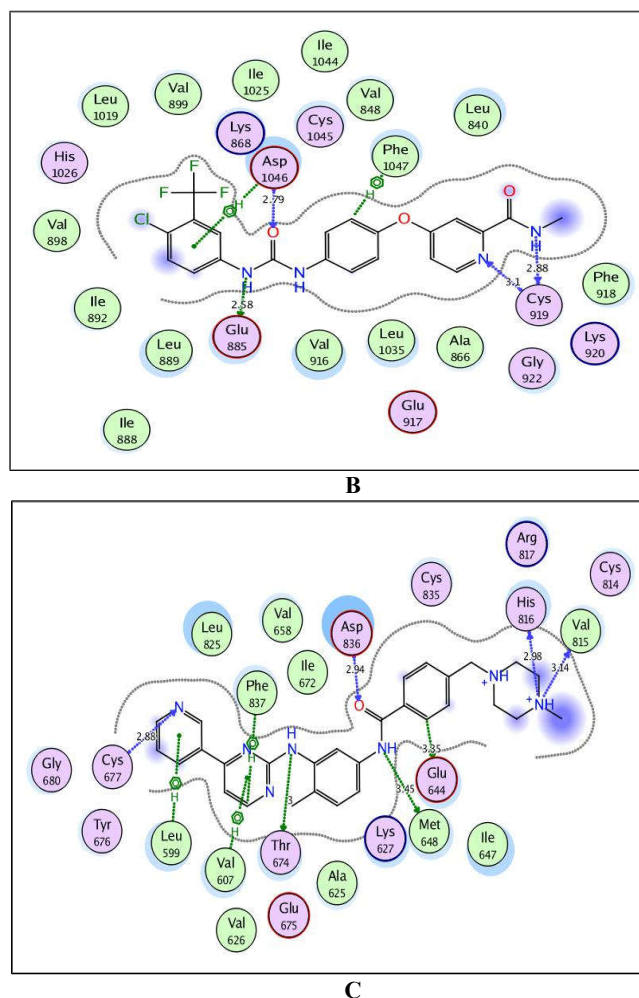
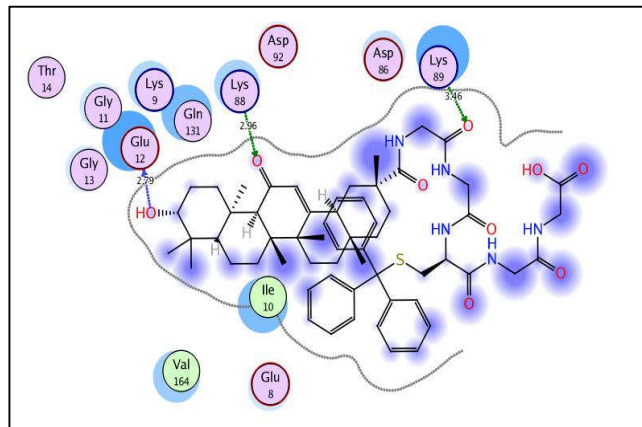
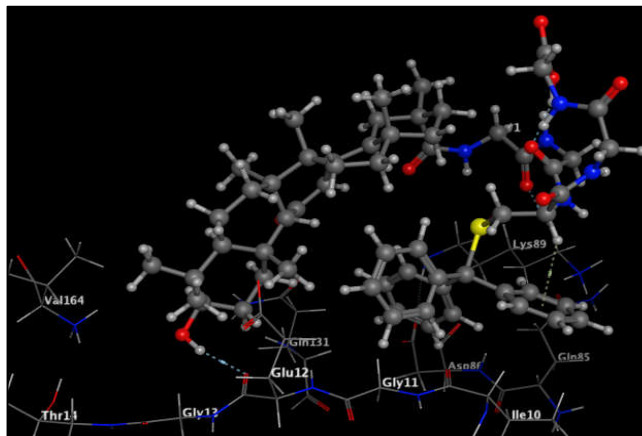


Figure 4. A, B, and C maps explore the 2D binding features of the native ligands, PY8, sorafenib, and imatinib within the active sites of CDK-2, VEGFR-2, and PDGFR- $\alpha$  (PDB codes: 2J9M, 4ASD, and 6JOL, respectively).

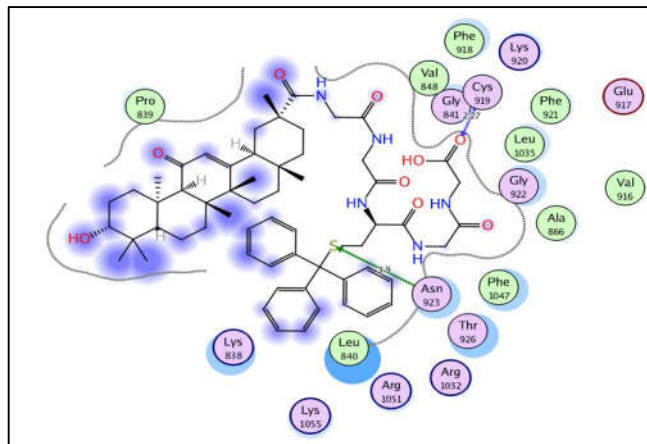
Docking of the newly synthesized candidate **6** within the active sites of CDK-2, VEGFR-2, and PDGFR- $\alpha$  afforded energy scores -9.73, -12.30, and -10.95 kcal/mol, respectively and its binding patterns were depicted in Figures 5, 6. It could be noted that the hydroxyl group at p-10 played an important role in fixation within the screened CDK-2 and PDGFR- $\alpha$  receptors through H-bond formation with Glu12 of CDK-2 (distance: 2.79 Å), and with Lys627 of PDGFR- $\alpha$  (distance: 2.87 Å). Moreover, two carbonyl oxygens promoted fitting and the inhibitory activity of compound **6** with CDK-2 through H-bonding with Asp88 and Lys89 (distance: 2.96 and 3.46 Å, respectively).



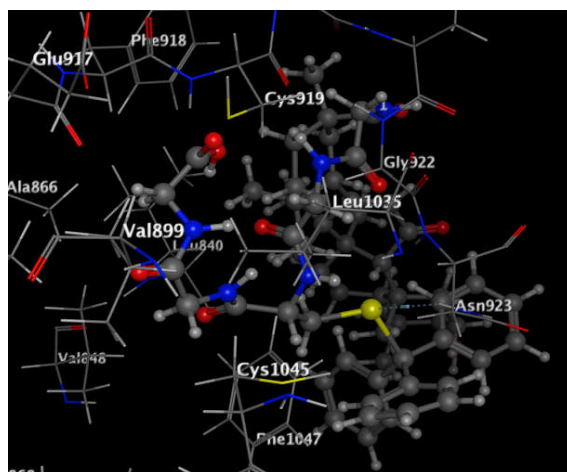
A



B



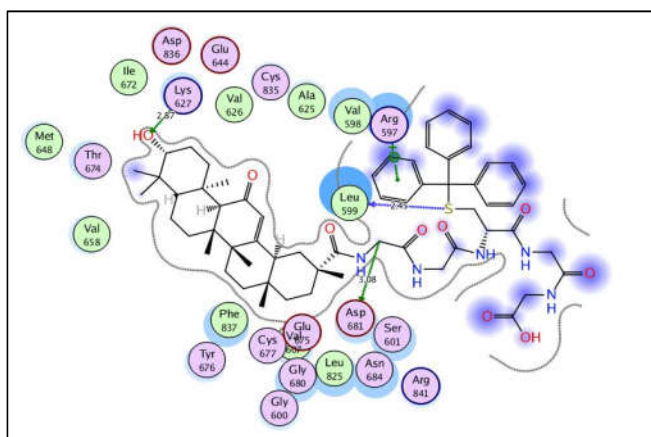
C



D

Figure 5. A and B; maps illustrate the 2D and 3D binding features of the promising target, **6** inside the binding site of CDK-2 (PDB code: 2J9M). C and D; maps illustrate the 2D and 3D binding features of the promising target, **2** inside the binding site of VEGFR-2 (PDB code: 4ASD).

The sulfur atom of *S*-tritylcysteinylglycylglycine potentiates fitting within ATP binding sites of VEGFR-2 and PDGFR- $\alpha$  through the formation of H-bonds with Asn923 and Leu599 (distance: 3.90 and 2.45 Å, respectively). The terminal carboxylic group showed an H-bond acceptor with the cornerstone of the essential amino acid Cys919 within the VEGFR-2 receptor (distance: 2.27 Å). Additionally, within PDGFR- $\alpha$ , there were H-bond and arene-cation interactions with Asp681 (distance: 3.08 Å) and Arg597, respectively. Finally and by focusing upon the superimposition views in Figure 7, the compound **6** bearing 18 $\beta$ -glycyrrhetic amide scaffold was well fitted and embedded nicely within the active sites of CDK-2, VEGFR-2, and PDGFR- $\alpha$  through different H-bond formation afforded from the hydroxyl group at p-10, sulfur atom of *S*-tritylcysteinylglycylglycine fragment and the terminal carboxylic group with the essential amino acids sharing the native ligands within the same vicinity of the screened enzymes.



A

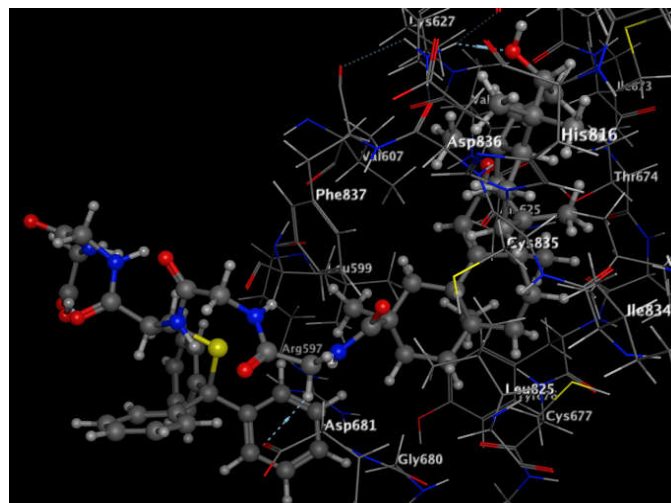
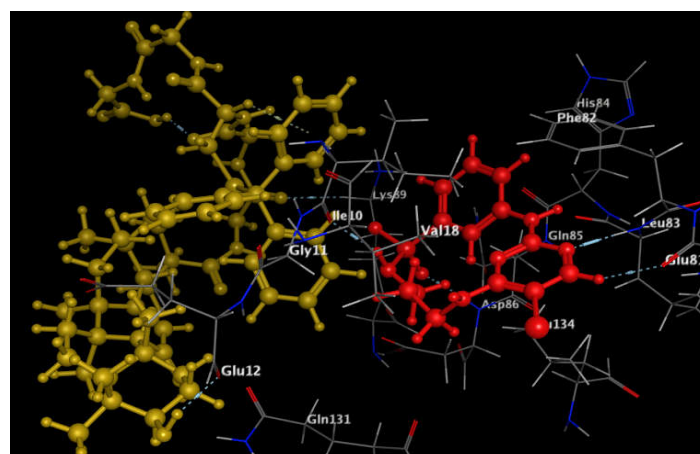
**B**

Figure 6. A and B maps illustrate the 2D and 3D binding features of the promising target, **6** inside the binding site of PDGFR- $\alpha$  (PDB code: 6JOL).

**A**

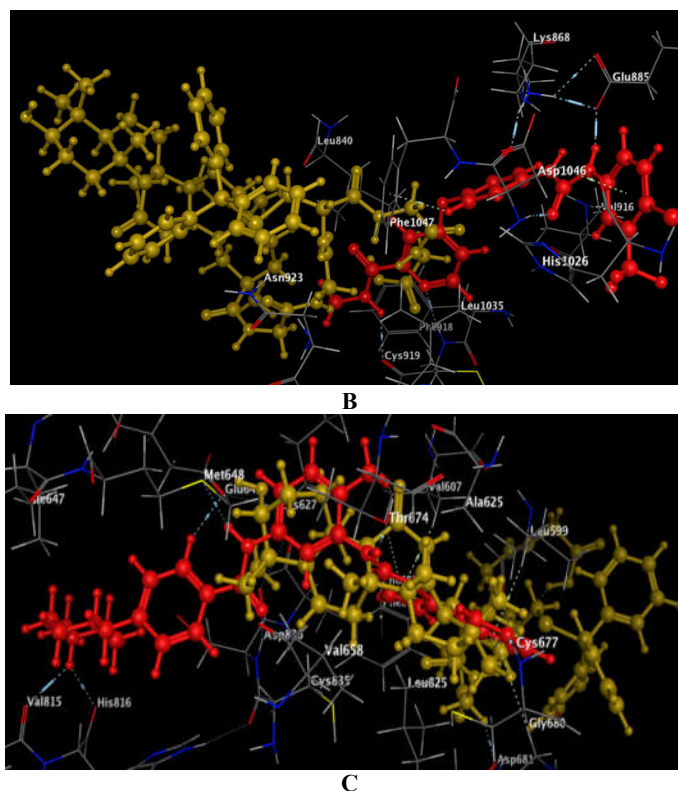


Figure 7. Maps A, B, and C illustrate the three-dimensional overlap between the potential target molecule (represented in yellow) and the initially docked ligands, namely PY8, sorafenib, and imatinib (depicted in red). This comparison is conducted within the active sites of CDK-2, VEGFR-2, and PDGFR- $\alpha$ , identified by their respective PDB codes: 2J9M, 4ASD, and 6JOL.

### CONCLUSION

This study involved creating and synthesizing novel peptides based on 18-glycyrrhetic acid (GA). The synthesis process followed conventional methods of peptide coupling in a liquid phase, combining GA with various amino acids to yield eight novel peptides labeled as **1–8**. All these new compounds were subjected to cytotoxicity testing to assess their potential using the MTT assay against *MCF-7*, *HCT-116*, and *HepG-2* cell lines. Among the tested peptides, namely **2**, **3**, **4**, **6**, and **7**, it was observed that they displayed significant cytotoxic effects against *MCF-7* and *HCT-116* cancer cells. In contrast, these peptides did not exhibit cytotoxicity against *HepG-2* liver cancer cells, with the exception of peptide **6**. Importantly, all the newly synthesized GA-peptides were found to be non-toxic to normal skin fibroblast cells (BJ-1). Additionally, when compared to the reference drug staurosporine, enzymatic assays demonstrated that peptides **2**, **4**, and **6** exhibited promising potential as multitargeting kinase inhibitors against CDK-2, VEGFR-2, and PDGFR- $\alpha$  kinases. Because target peptide **6** produced the most significant activities, it was chosen as a representative example to investigate its influence on the following cancer-related variables: Bax, BCL-2, p53, caspase-7, caspase-3, tubulin-B, and DNA fragmentation percentage. Furthermore, all of the new analogs appeared to be moderately active when tested versus a panel

of gram-negative and positive, as well as *Candida albicans*. To explain peptide 6's pharmacological efficacy, molecular docking experiments were also performed in order to determine how peptide 6 binds to the active sites of the three examined kinases, CDK-2, VEGFR-2, and PDGFR.

#### ACKNOWLEDGMENTS

Authors are grateful to King Saud University, Riyadh, Saudi Arabia for funding the work through Researchers Supporting Project No. (RSPD2024R852).

#### REFERENCES

- Bhattacharjee, S.; Bhattacharjee, A.; Majumder, S.; Majumdar, S.B.; Majumdar, S. Glycyrrhizic acid suppresses Cox-2-mediated anti-inflammatory responses during *Leishmania donovani* infection. *J. Antimicrob. Chemother.* **2012**, *67*, 1905-1914.
- Lin, S.C.; Chu, P.Y.; Liao, W.T.; Wu, M.Y.; Tsui, K.H.; Lin, L.T.; Huang, C.H.; Chen, L.L.; Li, C.J. Glycyrrhizic acid induces human MDA-MB-231 breast cancer cell death and autophagy via the ROS-mitochondrial pathway. *Oncol. Rep.* **2018**, *39*, 703-710.
- Su, X.; Wu, L.; Hu, M.; Dong, W.; Xu, M.; Zhang, P. Glycyrrhizic acid: a promising carrier material for anticancer therapy. *Biomed. Pharmacother.* **2017**, *95*, 670-678.
- Wang, H.; Ge, X.; Qu, H.; Wang, N.; Zhou, J.; Xu, W.; Xie, J.; Zhou, Y.; Shi, L.; Qin, Z.; Jiang, Z.; Yin, W.; Xia, J. Glycyrrhizic acid inhibits proliferation of gastric cancer cells by inducing cell cycle arrest and apoptosis. *Cancer Manag. Res.* **2020**, *12*, 2853-2861.
- Farooqui, A.; Khan, F.; Khan, I.; Ansari, I.A. Glycyrrhizin induces reactive oxygen species-dependent apoptosis and cell cycle arrest at G0/G1 in HPV18(+) human cervical cancer HeLa cell line. *Biomed. Pharmacother.* **2018**, *97*, 752-764.
- Moustafa, G.O.; Shalaby, A.; Naglah, A.M.; Mounier, M.M.; El-Sayed, H.; Anwar, M.M.; Nossier, E.S. Synthesis, characterization, in vitro anticancer potentiality, and antimicrobial activities of novel peptide-glycyrrhetic-acid-based derivatives. *Molecules* **2021**, *26*, 4573.
- Wang, X.F.; Zhou, Q.M.; Lu, Y.Y.; Zhang, H.; Huang, S.; Su, S.B. Glycyrrhetic acid potently suppresses breast cancer invasion and metastasis by impairing the p38 MAPK-AP1 signaling axis. *Expert Opin. Biol. Ther.* **2015**, *19*, 577-587.
- Irshad, R.; Raj, N.; Gabr, G.A.; Manzoor, N.; Husain, M. Integrated network pharmacology and experimental analysis unveil multi-targeted effect of 18 $\alpha$ -glycyrrhetic acid against non-small cell lung cancer. *Front. Pharmacol.* **2022**, *13*, 1018974.
- Juin, S.K.; Ghosh, S.; Majumdar, S. Glycyrrhizic acid facilitates anti-tumor immunity by attenuating Tregs and MDSCs: An immunotherapeutic approach. *Int. Immunopharmacol.* **2020**, *88*, 106932.
- Liu, B.; Qu, L.; Yan S. Cyclooxygenase-2 promotes tumor growth and suppresses tumor immunity. *Cancer Cell Int.* **2015**, *15*, 106.
- Jina, L.; Daib, L.; Jia, M.; Wang, H. Mitochondria-targeted triphenylphosphonium conjugated glycyrrhetic acid derivatives as potent anticancer drugs. *Bioorg. Chem.* **2019**, *85*, 179-190.
- Huang, M.; Gong, P.; Wang, Y.; Xie, X.; Ma, Z.; Xu, Q.; Liua, D.; Jing, Y.; Zhao, L. Synthesis and antitumor effects of novel 18 $\beta$ -glycyrrhetic acid derivatives featuring an exocyclic  $\alpha$ ,  $\beta$ -unsaturated carbonyl moiety in ring A. *Bioorg. Chem.* **2020**, *103*, 104187.
- Hoenke, S.; Serbian, I.; Deigner, H.P.; Csuk, R. Mitocanic di- and triterpenoid rhodamine B conjugates. *Molecules* **2020**, *25*, 5443.
- Shanmugam, M.K.; Dai, X.; Kumar, A.P.; Tan, B.K.; Sethi, G.; Bishayee, A. Oleanolic acid and its synthetic derivatives for the prevention and therapy of cancer: preclinical and clinical evidence. *Cancer Lett.* **2014**, *346*, 206-216.
- Chintharlapalli, S.; Papineni, S.; Jutooru, I.; McAlees, A.; Safe, S. Structure-dependent activity of glycyrrhetic acid derivatives as peroxisome proliferator-activated receptor gamma agonists in colon cancer cells. *Mol. Cancer Ther.* **2007**, *6*, 1588-1598.

16. Chadalapaka, G.; Jutooru, I.; McAlees, A.; Stefanac, T.; Safe, S. Structure-dependent inhibition of bladder and pancreatic cancer cell growth by 2-substituted glycyrrhetic and ursolic acid derivatives. *Bioorg. Med. Chem. Lett.* **2008**, *18*, 2633-2639.
17. Gong, P.; Li, K.; Li, Y.; Liu, D.; Zhao, L.; Jing, Y. HDAC and Ku70 axis- an effective target for apoptosis induction by a new 2-cyano-3-oxo-1,9-dien glycyrrhetic acid analogue. *Cell Death Dis.* **2018**, *9*, 623-634.
18. Ling, Z.N.; Jiang, Y.F.; Ru, J.N.; Lu, J.H.; Ding, B.; Wu, J. Amino acid metabolism in health and disease. *Sig. Transduct. Targe. Ther.* **2023**, *8*, 345.
19. Castagnolo, D. Looking back and moving forward in medicinal chemistry. *Nat. Commun.* **2023**, *14*, 4299.
20. Moustafa, G.O. Synthesis of dibenzofuran derivatives possessing anti-bacterial activities. *Egypt. J. Chem.* **2021**, *64*, 2075-2093.
21. Khalaf, H.S.; Naglah, A.M.; Al-Omar, M.A.; Moustafa, G.O.; Awad, H.M.; Bakheit, A.H. Synthesis, docking, computational studies, and antimicrobial evaluations of new dipeptide derivatives based on nicotinoylglycylglycine hydrazide. *Molecules* **2020**, *25*, 3589.
22. Al-Wasidi, A.S.; Naglah, A.; Kalmouch, A.; Adam, A.M.A.; Refat, M.; Moustafa, G.O. Preparation of Cr<sub>2</sub>O<sub>3</sub>, MnO<sub>2</sub>, Fe<sub>2</sub>O<sub>3</sub>, NiO, CuO, and ZnO oxides using their glycine complexes as precursors for in situ thermal decomposition. *Egypt. J. Chem.* **2020**, *63*, 1109-1118.
23. Moustafa, G.O. Therapeutic potentials of cyclic peptides as promising anticancer drugs. *Egypt. J. Chem.* **2021**, *64*, 1777-1787.
24. Naglah, A.M.; Moustafa, G.O.; Elhenawy, A.A.; Mounier, M.M.; El-Sayed, H.; Al-Omar, M.A.; Almhizia, A.A.; Bhat, M.A. N<sup>α</sup>-1,3-Benzenedicarbonyl-bis-(amino acid) and dipeptide candidates: Synthesis, cytotoxic, antimicrobial and molecular docking investigation. *Drug Des. Devel. Ther.* **2021**, *15*, 1315-1332.
25. Moustafa, G.O.; Younis, A.; Al-Yousef, S.A.; Mahmoud, S.Y. Design, synthesis of novel cyclic pentapeptide derivatives based on 1,2-benzenedicarbonyl chloride with expected anticancer activity. *J. Comput. Theor. Nanos.* **2019**, *16*, 1733-1739.
26. Abo-Ghalia, M.H.; Moustafa, G.O.; Amr, A.E.; Naglah, A.M.; Elsayed, E.A.; Bakheit, A.H. Anticancer activities of newly synthesized chiral macrocyclic heptapeptide candidates. *Molecules* **2020**, *25*, 1253.
27. Kalmouch, A.; Rdwan, M.; Omran, M.; Sharaky, M.; Moustafa, G.O. Synthesis of novel 2, 3'-bipyrrole derivatives from chalcone and amino acids as antitumor agents. *Egypt. J. Chem.* **2020**, *63*, 4409-4421.
28. Abd El-Meguid, E.A.; Naglah, A.M.; Moustafa, G.O.; Awad, H.M.; El Kerdawy, A.M. Novel benzothiazole-based dual VEGFR-2/EGFR inhibitors targeting breast and liver cancers: Synthesis, cytotoxic activity, QSAR and molecular docking studies. *Bioorg. Med. Chem. Lett.* **2022**, *58*, 128529.
29. Moustafa, G.O.; Sabry, E.; Zayed, E.M.; Mohamed, G.G. Structural characterization, spectroscopic studies, and molecular docking studies on metal complexes of new hexadentate cyclic peptide ligand. *Appl. Organomet. Chem.* **2022**, *36*, e6515.
30. Moustafa, G.O.; Al-Wasidi, A.S.; Naglah, A.M.; Refat, M. Synthesis of dibenzofuran derivatives possessing anticancer activities: A review. *Egypt. J. Chem.* **2020**, *63*, 2355-2367.
31. Mohamed, F.H.; Shalaby, A.; Abdelazem, A.; Mounier, M.; Nossier, E.S.; Moustafa, G.O. Design, synthesis and molecular docking studies of novel cyclic pentapeptides based on phthaloyl chloride with expected anticancer activity. *Egypt. J. Chem.* **2020**, *63*, 1723-1736.
32. Bhattacharya, B.; Mukherjee, S. Cancer therapy using antibiotics. *J. Cancer Res. Ther.* **2015**, *6*, 849-858.
33. Zaman, S.; Wang, R.; Gandhi, V. Targeting the apoptosis pathway in hematologic malignancies. *Leuk. Lymphoma.* **2014**, *55*, 1980-1992.

34. Othman, I.M.; Gad-Elkareem, M.A.; Amr, A.E.; Al-Omar, M.A.; Nossier, E.S.; Elsayed, E.A. Novel heterocyclic hybrids of pyrazole targeting dihydrofolate reductase: design, biological evaluation and in silico studies. *J. Enzyme Inhib. Med. Chem.* **2020**, *35*, 1491-1502.
35. Othman, I.M.; Alamshany, Z.M.; Tashkandi, N.Y.; Gad-Elkareem, M.A.; Anwar, M.M.; Nossier, E.S. New pyrimidine and pyrazole-based compounds as potential EGFR inhibitors: Synthesis, anticancer, antimicrobial evaluation and computational studies. *Bioorg. Chem.* **2021**, *114*, 105078.
36. Abd El-Meguid, E.A.; El-Deen, E.M.M.; Moustafa, G.O.; Awad, H.M.; Nossier, E.S. Synthesis, anticancer evaluation and molecular docking of new benzothiazole scaffolds targeting FGFR-1. *Bioorg. Chem.* **2022**, *119*, 105504.
37. Li, Y.; Tan, C.; Gao, C.; Zhang, C.; Luan, X.; Chen, X.; Liu, H.; Chen, Y.; Jiang, Y. Discovery of benzimidazole derivatives as novel multi-target EGFR, VEGFR-2 and PDGFR kinase inhibitors. *Bioorg. Med. Chem.* **2011**, *19*, 4529-4535.
38. Kaur, R.; Kaur, G.; Gill, R.K.; Soni, R.; Bariwal, J. Recent developments in tubulin polymerization inhibitors: An overview. *Eur. J. Med. Chem.* **2014**, *87*, 89-124.
39. Kenta, T.; and Goshima, G. Microtubule-associated proteins promote microtubule generation in the absence of  $\gamma$ -tubulin in human colon cancer cells. *J. Cell Biol.* **2021**, *220*, e202104114.
40. Al-Wasidi, A.S.; Naglah, A.M.; Refat, M.; El-Megharbel, S.M.; Kalmouch, A.; Moustafa, G.O. Synthesis, spectroscopic characterization and antimicrobial studies of Mn(II), Co(II), Ni(II), Cr(III) and Fe(III) melatonin drug complexes. *Egypt. J. Chem.* **2020**, *63*, 1469-1481.
41. Rodriguez-Nava, G.; Mohamed, A.; Yanez-Bello, M.A.; Trelles-Garcia, D.P. Advances in medicine and positive natural selection: Prosthetic valve endocarditis due to biofilm producer *Micrococcus luteus*. *ID Cases.* **2020**, *20*, e00743.
42. Elmorsy, M.R.; Abdel-Latif, E.; Gaffer, H.E.; Mahmoud, S.E. Fadda, A.A. Anticancer evaluation and molecular docking of new pyridopyrazolo-triazine and pyridopyrazolo-triazole derivatives. *Sci. Rep.* **2023**, *13*, 2782.
43. Amr, A.E.; El-sayed, E.A.; Al-Omar, M.A., Badr Eldin, H.O.; Nossier, E.S.; Abdallah, M.M. Design, synthesis, anticancer evaluation and molecular modeling of novel estrogen derivatives. *Molecules* **2019**, *24*, 416.
44. Ali, I.H.; Abdel-Mohsen, H.T.; Mounier, M.M.; Abo-Elfadl, M.T.; El Kerdawy, A.M.; Ghannam, I.A. Design, synthesis and anticancer activity of novel 2-arylbenzimidazole/2-thiopyrimidines and 2-thioquinazolin-4 (3H)-ones conjugates as targeted RAF and VEGFR-2 kinases inhibitors. *Bioinorg. Chem.* **2022**, *126*, 105883.
45. Barbareschi, M.; Caffo, O.; Veronese, S.; Leek, R.D.; Fina, P.; Fox, S.; Pezzella, F. Bcl-2 and p53 expression in node-negative breast carcinoma: a study with long-term follow-up. *Hum. Pathol.* **1996**, *27*, 1149-1155.
46. Onur, R.; Semerciöz, A.; Orhan, I.; Yekeler, H. The effects of melatonin and the antioxidant defense system on apoptosis regulator proteins (Bax and Bcl-2) in experimentally induced varicocele. *Urol. Res.* **2004**, *32*, 204-208.
47. Thomas, M.D.; McIntosh, G.G.; Anderson, J.J.; McKenna, D.M.; Parr, A.H.; Johnstone, R.; Lennard, T.W.; Horne, C.H.; Angus, B. A novel quantitative immunoassay system for p53 using antibodies selected for optimum designation of p53 status. *J. Clin. Pathol.* **1997**, *50*, 143-147.
48. El-Sayed, W.A.; Alminderej, F.M.; Mounier, M.M.; Nossier, E.S.; Saleh, S.M.; Kassem, A.F. Novel 1, 2, 3-Triazole-coumarin hybrid glycosides and their tetrazolyl analogues: design, anticancer evaluation and molecular docking targeting EGFR, VEGFR-2 and CDK-2. *Molecules* **2022**, *27*, 2047.
49. Liliom, K.; Lehotzky, A.; Molnar, A.; Ovadi, J. Characterization of tubulin-alkaloid interactions by enzyme-linked immunosorbent assay. *Anal. Biochem.* **1995**, *228*, 18-26.
50. Burton, K. A study of the conditions and mechanism of the diphenylamine reaction for the colorimetric estimation of deoxyribonucleic acid. *Biochem. J.* **1956**, *62*, 315-323.